Nuclear Instruments and Methods in Physics Research B 383 (2016) 191–212

Contents lists available at ScienceDirect

Nuclear Instruments and Methods in Physics Research B

journal homepage: www.elsevier.com/locate/nimb

New excitation functions for proton induced reactions on natural titanium, nickel and copper up to 70 MeV

E. Garrido [a], C. Duchemin [a,*], A. Guertin [a], F. Haddad [a,b], N. Michel [a,b], V. Métivier [a]

[a] SUBATECH, Ecole des Mines de Nantes, Université de Nantes, CNRS/IN2P3, Nantes, France
[b] GIP Arronax, 1 rue Aronnax, 44817 Saint-Herblain, France

ARTICLE INFO

Article history:
Received 19 May 2016
Received in revised form 13 July 2016
Accepted 15 July 2016

Keywords:
Stacked-foil technique
ARRONAX cyclotron
70 MeV proton beam
Titanium
Nickel
Copper
TALYS 1.6

ABSTRACT

New excitation functions for proton induced nuclear reactions on natural titanium, nickel and copper were measured, using the stacked-foil technique and gamma spectrometry, up to 70 MeV. The experimental cross sections were measured using the Ti-nat(p,x) V-48, Ni-nat(p,x) Ni-57 and Cu-nat(p,x) Zn-62,Co-56 monitor reactions recommended by the International Atomic Energy Agency (IAEA), depending on the investigated energy range. Data have been extracted for the Ti-nat(p,x) Sc-43,44m,46,47,48, V-48, K-42,43, Ni-nat(p,x) Ni-56,57, Co-55,56,57,58, Mn-52,54, Cu-nat(p,x) Cu-61,64, Ni-57, Co-56,57,58,60, Zn-62,65, Mn-54 reactions. Our results are discussed and compared to the existing ones as well as with the TALYS code version 1.6 calculations using default models. Our experimental data are in overall good agreement with the literature. TALYS is able to reproduce, in most cases, the experimental trend. Our new experimental results allow to expand our knowledge on these excitation functions, to confirm the existing trends and to give additional values on a large energy range. This work is in line with the new Coordinated Research Project (CRP) launched by the IAEA to expand the database of monitor reactions.

1. Introduction

Our researches are focused on radionuclide production mainly for medical applications, either for therapy or diagnostics. This work is conducted in close collaboration with the GIP ARRONAX that possesses a high energy and high intensity multi-particles cyclotron. In this frame, data were measured for alpha emitters, such as the U-230/Th-226, Th-227/Ra-223 and Ac-225/Bi-213 generators, with protons up to 70 MeV [15]. In this context, several stack of thin foils were irradiated in order to limit the energy uncertainties and ensure the reproducibility of our values. Some monitor foils, made of copper, titanium or nickel, were placed in each stack to quantify the particle beam flux all along the stack. From these irradiated materials, new experimental cross section data have been extracted which allow to expand our knowledge on these excitation functions, to confirm the existing trends and to give additional values on a wider energy range. The data presented in this article are coming from several experiments performed at different dates between February 2014 and December 2015.

In this work, we measured data up to 70 MeV for the Ti-nat(p,x) Sc-43,44m,46,47,48, V-48, K-42,43, Ni-nat(p,x) Ni-56,57, Co-55,56,57,58, Mn-52,54 and Cu-nat(p,x) Cu-61,64, Ni-57, Co-56,57,58,60, Zn-62,65, Mn-54 reactions.

Some of these data are of interest for medical applications and/or monitor reactions. Indeed, Sc-43 and Sc-44 are useful for nuclear imaging [29,16], Sc-47 for therapy [41]. Co-55 and Mn-52 are of interest for diagnostics [6,31,14,62]. Several copper radionuclides are suitable for PET imaging [66] as Cu-61 and Cu-64. Data on Zn-62 [50] are also of interest since Cu-62 can be produced via its decay. As Cu-64 is a β+ emitter and a $\beta-$ emitter, it is well suitable for PET imaging [5] but also for dosimetry and potentially also for therapy [12]. In addition, the IAEA have launched a Coordinated Research Project (CRP) in 2012 to get additional data for monitor reactions and medical isotope production [49]. A requirement list has been set, including the Ti-nat(p,x) Sc-46, Ni-nat(p,x) Co-56, Co-58,Ni-57, Cu-nat(p,x) Co-58,Zn-62,Zn-65 reactions that have been investigated in this work.

2. Materials and methods

2.1. Experimental set-up and data measurements

The production cross section data were obtained using the stacked-foils method [15,9], which consists in the irradiation of a set of thin foils followed by gamma spectrometry measurements to assess the produced activity of the investigated radionuclide.

* Corresponding author.
E-mail address: Charlotte.Duchemin@subatech.in2p3.fr (C. Duchemin).

http://dx.doi.org/10.1016/j.nimb.2016.07.011
0168-583X/

Table 1
Isotopic composition of the natural foils from Goodfellow®.

Ti-nat	Ti-46	Ti-47	Ti-48	Ti-49	Ti-50
	8.0%	7.5%	73.7%	5.5%	5.3%
Ni-nat	Ni-58	Ni-60	Ni-61	Ni-62	Ni-64
	68.27%	26.10%	1.13%	3.59%	0.91%
Cu-nat	Cu-63	Cu-65			
	69.2%	30.8%			

Our experiments were carried out at the ARRONAX cyclotron (Nantes, France), in the AX hall devoted to experiments in physics, radiolysis and radiobiology [23].

Each thin foil was weighed before irradiation using an accurate scale ($\pm 10^{-5}$ g) and scanned to precisely determine its area. From these values and assuming that the thickness is homogeneous over the whole surface, the thickness was deduced: around 20 μm for the titanium and copper foils and 25 μm for the nickel foils. All foils were purchased from Goodfellow® with high isotopic and chemical purity: 99.6% for titanium, 99% for nickel and 99.9% for copper. Their isotopic composition is reported in Table 1.

The incident beam energy was fixed by the setting parameters of the cyclotron with an uncertainty, defined by the cyclotron provider and based on simulations, of ±0.5 MeV. This energy determination has been validated with previous work and has given data

Table 2
Physical characteristics of the radionuclides produced in titanium [36,17] and reaction thresholds [51].

Radioisotope	$T_{1/2}$	E_γ (keV)	I_γ (%)	Contributing reactions	Threshold (MeV)
Sc-43	3.891 (12) h	372.9	23	Ti-46(p,α)	3.14
				Ti-46(p,n+He-3)	24.17
				Ti-46(p,2n+2p)	32.06
				Ti-47(p,n+α)	12.21
				Ti-47(p,2n+He-3)	33.23
				Ti-47(p,3n+2p)	41.11
				Ti-48(p,2n+α)	24.08
				Ti-48(p,3n+He-3)	45.09
				Ti-48(p,4n+2p)	52.97
				Ti-49(p,3n+α)	32.38
				Ti-49(p,4n+He-3)	53.38
				Ti-49(p,5n+2p)	61.26
				Ti-50(p,4n+α)	43.52
				Ti-50(p,5n+He-3)	64.52
Sc-44m	58.6 (1) h	271.13	86.7 (3)	Ti-46(p,He-3)	14.26
				Ti-46(p,2p+n)	22.15
				Ti-47(p,α)	2.30
				Ti-47(p,2p+2n)	31.21
				Ti-48(p,α+n)	14.17
				Ti-48(p,2p+3n)	43.06
				Ti-49(p,α+2n)	22.48
				Ti-49(p,2p+4n)	51.36
				Ti-50(p,α+3n)	32.28
				Ti-50(p,2p+5n)	61.26
Sc-46	83.79 (4) d	889.277	99.984 (1)	Ti-47(p,2p)	10.69
		1120.545	99.987 (1)	Ti-48(p,He-3)	14.68
				Ti-48(p,2p+n)	22.56
				Ti-49(p,α)	1.98
				Ti-49(p,2p+2n)	30.86
				Ti-50(p,α+n)	13.14
				Ti-50(p,2p+3n)	42.00
Sc-47	3.3492 (6) d	159.377	68.3 (4)	Ti-48(p,2p)	11.69
				Ti-49(p,He-3)	12.11
				Ti-49(p,2p+n)	19.99
				Ti-50(p,α)	2.28
				Ti-50(p,2p+2n)	31.14
Sc-48	43.67 (9) h	175.361	7.48 (9)	Ti-49(p,2p)	11.58
		1037.599	97.6 (5)	Ti-50(p,He-3)	14.86
				Ti-50(p,2p+n)	22.73
V-48	15.9735 (25) d	944.104	7.76 (9)	Ti-48(p,n)	4.90
		983.517	99.98 (20)	Ti-49(p,2n)	13.21
		1312.096	97.5 (8)	Ti-50(p,3n)	23.97
K-42	12.360 (3) h	1524.7	18	Ti-46(p,2p+He-3)	32.01
				Ti-46(p,4p+n)	39.90
				Ti-47(p,2p+α)	20.05
				Ti-47(p,4p+2n)	48.95
				Ti-48(p,2p+α+n)	31.91
				Ti-48(p,4p+3n)	60.80
				Ti-49(p,2p+α+2n)	40.21
				Ti-49(p,4p+4n)	69.09
K-43	22.3 (1) h	372.76	87	Ti-46(p,4p)	30.06
		396.86	11.85 (8)	Ti-47(p,2p+He-3)	31.24
		593.39	11.26 (8)	Ti-47(p,4p+n)	39.12
		617.49	76.2 (6)	Ti-48(p,2p+α)	22.08
				Ti-48(p,4p+2n)	50.97
				Ti-49(p,2p+α+n)	30.39
				Ti-49(p,4p+3n)	59.26

in good agreement with the literature for a wide range of target masses over a wide incident energy range. The beam line is under vacuum and closed using a 75 μm thick kapton foil. The stacks were located about 6.8 cm downstream in air. The energy through each thin foil was determined in the middle of the foil using the SRIM software [69]. Energy losses in the kapton foil and air were taken into account. Aluminum and copper degrader foils, from 100 μm to 1 mm thick, were used to decrease the energy beam all along the stack. Depending on the number of foils, the energy uncertainty increases up to ±2.0 MeV due to spatial and energy straggling and the initial energy beam spread. Typical irradiations were carried out with about 100 nA during 30 min [15].

The particle flux through the stack was quantified using monitor reactions suggested by the IAEA [59]; Ti-nat(p,x) V-48 reaction up to 20 MeV, Ni-nat(p,x) Ni-57 reaction between 20 MeV and 46 MeV, Cu-nat(p,x) Zn-62 reaction between 46 MeV and 60 MeV, and the Cu-nat(p,x) Co-56 reaction above 60 MeV.

During the irradiation, an instrumented beam stop is used to control the beam current stability. It can not be used as Faraday cup since it is not equipped with an electron suppression device, which is required for a precise beam current measurement. However, using the number of charges collected with the instrumented beam stop, the cross section values have been found in agreement within 5% in average with those presented in this article and obtained using monitor reactions.

After some cooling time (around 14 h after the end of irradiation), activity measurements were performed using a high purity germanium detector, with low-background lead and copper shield, from Canberra®. Gamma spectra were recorded using the LVis software from Ortec® in a suitable geometry previously

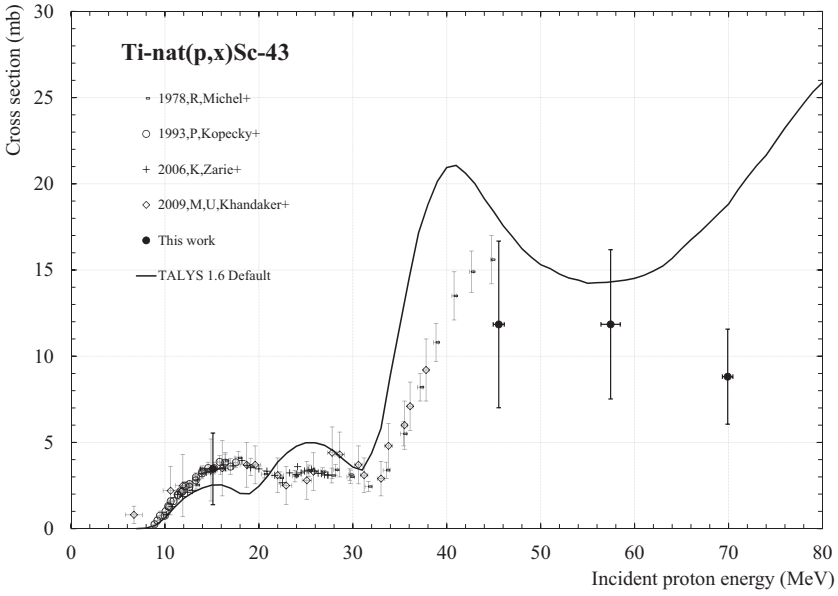

Fig. 1. Ti-nat(p,x) Sc-43 excitation function. (See above-mentioned references for further information.)

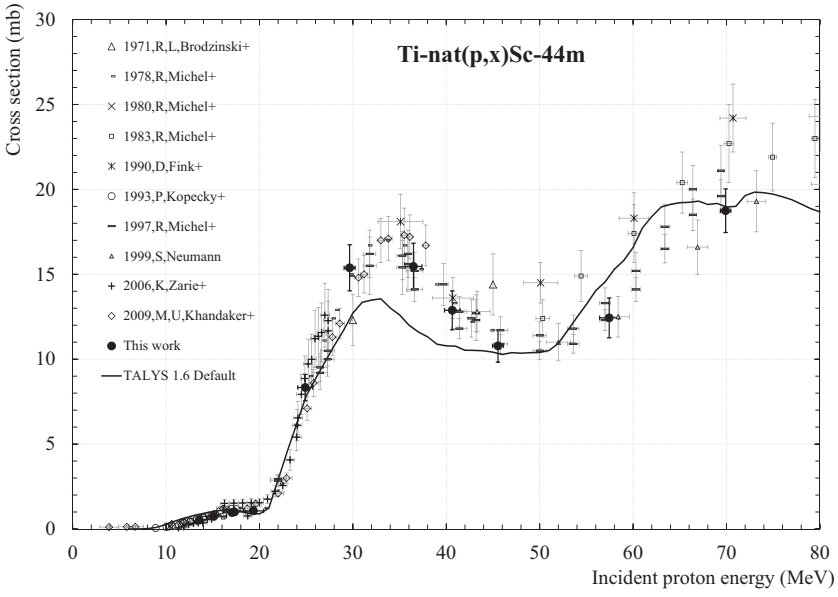

Fig. 2. Ti-nat(p,x) Sc-44m excitation function. (See above-mentioned references for further information.)

calibrated with standard γ sources (Co-57,60 and Eu-152) from Lea Cerca (France).

Samples were placed at a height of 19 cm from the detector in order to reduce the dead time and the effect of sum peaks. The dead time during measurements was always kept below 10%.

The activity values of the produced radionuclides were derived from the spectra and libraries containing the nuclear decay data given in Tables 2, 4 and 6, using the FitzPeaks Gamma Analysis and Calibration Software (JF Computing Services). All foils were counted three times. The first activity measurements were performed for one hour, the day after irradiation; the second ones were started one week later, with a counting time between 24 h and 60 h. Third measurements were performed to validate the activity values obtained with the two other measurements, to get the activity of some radionuclides after the decay of their parents and to measure long lived radionuclides.

2.2. Cross section calculation

Knowing the precise thickness of the foil and the total activity of each radionuclide produced in the target, their production cross section are calculated using the activation formula (1) with the appropriate particle flux.

$$\sigma(E) = \frac{\mathrm{Act} \cdot \mathrm{A}}{\chi \cdot \Phi \cdot \mathrm{N}_a \cdot \mathrm{M} \cdot (1 - \exp^{-\lambda t})} \quad (1)$$

In Eq. (1), the production cross section σ (mb) of a radionuclide at a given energy, E, depends on its measured activity corrected to the time at the end of irradiation Act (Bq), its decay constant $\lambda(s^{-1})$, its atomic mass A ($g{\cdot}mol^{-1}$), its areal density M ($g{\cdot}cm^{-2}$), its chemical purity and isotopic abundance χ, the Avogadro constant (N_a, the irradiation duration t (s) and the beam current Φ ($p{\cdot}s^{-1}$).

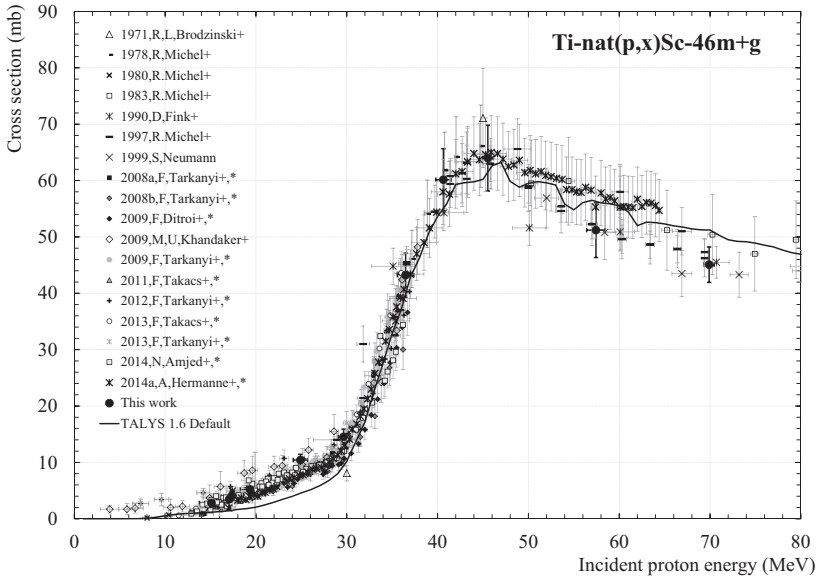

Fig. 3. Ti-nat(p,x) Sc-46m+g excitation function. (See above-mentioned references for further information.)

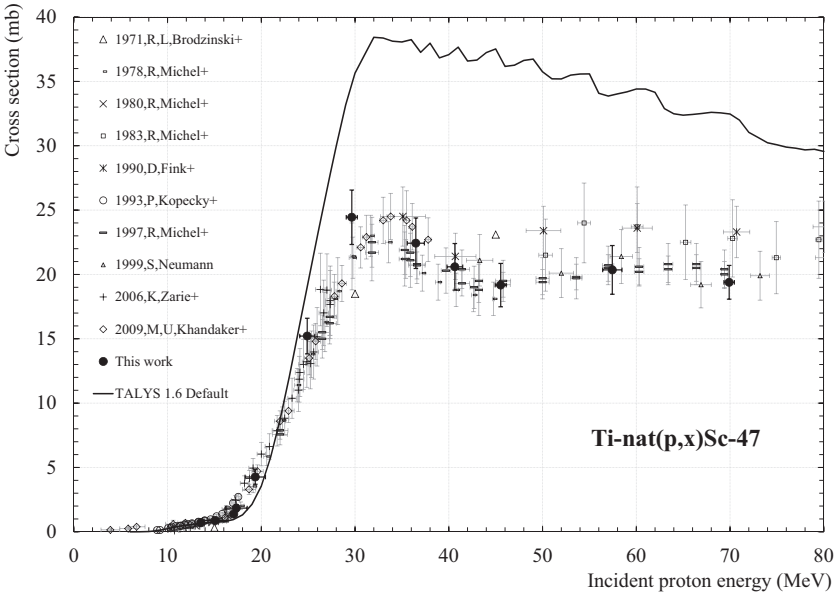

Fig. 4. Ti-nat(p,x) Sc-47 excitation function. (See above-mentioned references for further information.)

In our experiment, and because we use thin foils, each one receives the same beam current as the monitor foil that follows. It is then possible to define a relative Eq. (2) in which the knowledge of the beam current is no longer necessary. In this equation, the prime parameters are associated with the radionuclide used as monitor, while the others relate to the radionuclide for which the cross section is investigated.

$$\sigma(E) = \sigma'(E') \cdot \frac{\chi' \cdot \mathrm{Act} \cdot \mathrm{A} \cdot \mathrm{M}' \cdot (1 - \exp^{-\lambda' t})}{\chi \cdot \mathrm{Act}' \cdot \mathrm{A}' \cdot \mathrm{M} \cdot (1 - \exp^{-\lambda t})} \quad (2)$$

The cross section uncertainty is estimated with a propagation error calculation. Since all the parameters of Eq. (2) are independent, the total error is expressed as a quadratic sum (see Eq. (3)).

$$\frac{\Delta\sigma}{\sigma} = \sqrt{\left(\frac{\Delta\sigma'}{\sigma'}\right)^2 + \left(\frac{\Delta\mathrm{Act}}{\mathrm{Act}}\right)^2 + \left(\frac{\Delta\mathrm{Act}'}{\mathrm{Act}'}\right)^2 + \left(\frac{\Delta\mathrm{M}}{\mathrm{M}}\right)^2 + \left(\frac{\Delta\mathrm{M}'}{\mathrm{M}'}\right)^2} \quad (3)$$

Main uncertainties come from the measured activities (less than 10% in most cases), the areal density of the foils (around 1%) and the uncertainty on the recommended cross section values. Since no uncertainty is given for the recommended cross section values, we have decided to use the uncertainty of the nearest experimental value used by the IAEA to perform the adjustment. It leads to an uncertainty of 8% in average. The contribution of the uncertainty on the irradiation time is not significant and has been neglected.

2.3. Comparison with the TALYS 1.6 code

The cross section values, shown in Figs. 1–26, are compared to the TALYS code version 1.6 released in December, 2013 [37]. TALYS is a nuclear reaction program to simulate reaction induced by light particles on nuclei heavier than carbon. It incorporates many

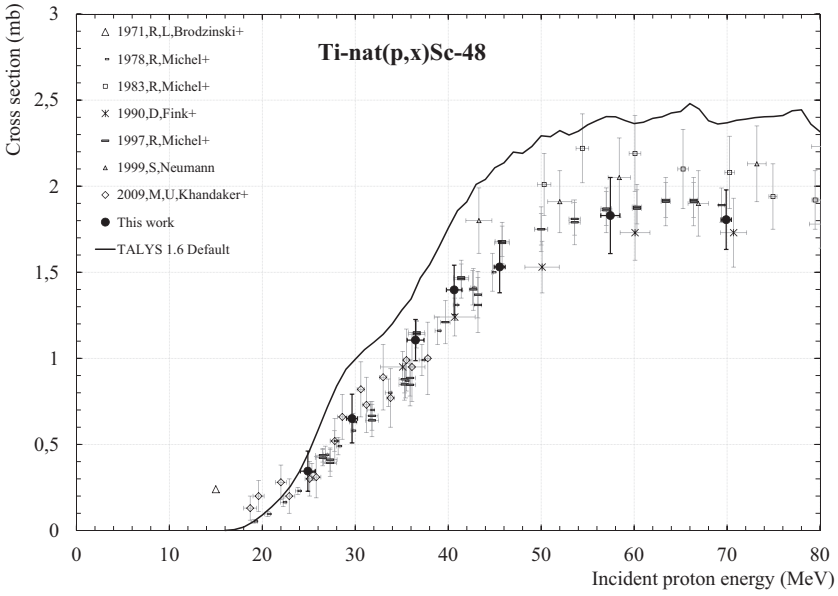

Fig. 5. Ti-nat(p,x) Sc-48 excitation function. (See above-mentioned references for further information.)

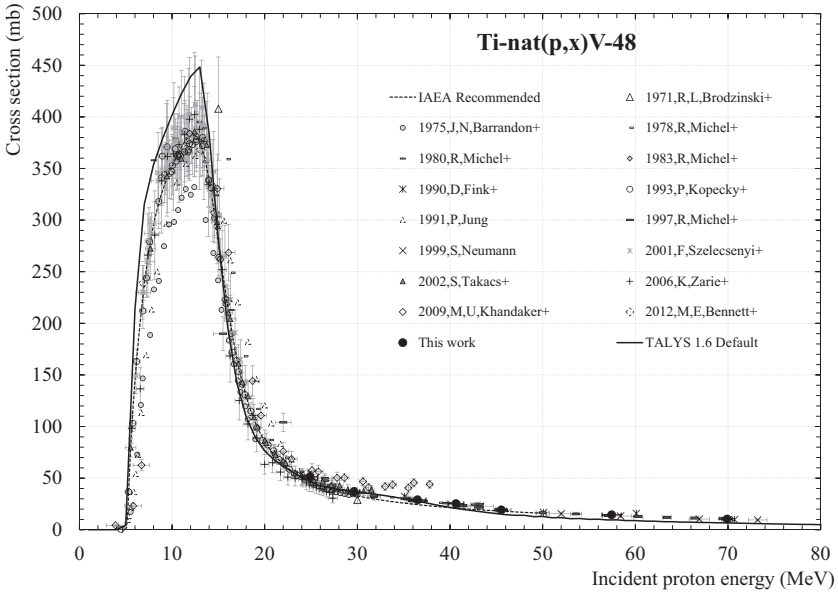

Fig. 6. Ti-nat(p,x) V-48 excitation function. (See above-mentioned references for further information.)

theoretical models to predict observables including theoretical cross section values as a function of the incident particle energy (from 1 keV to 1 GeV). A combination of models that better describes the whole set of available data for all combination of projectiles, targets and incident energies have been defined by the authors and put as default in the code. This way, the code can be executed with an input file that contains a minimal set of information: the projectile type and its incident energy, the target type and its mass. The experimental data obtained in this work are compared to TALYS with default models.

3. Results and discussions

Our production cross section values, obtained via a relative calculation using the recommended monitor reactions stated in the previous section, are presented in Tables 3, 5 and 7. Our results are plotted as full circles in Figs. 1–26.

3.1. Proton induced reactions on natural titanium

In this part, the production cross sections values of vanadium, scandium and potassium radionuclides induced by protons interacting with natural titanium are shown. No data for the Ti-nat(p, x) V-48 reaction has been obtained under 20 MeV, where it was used as monitor. The physical characteristics of the investigated radionuclides are summarized in Table 2 and the associated production cross section numerical values are presented in Table 3.

3.1.1. Production of Sc-43

Sc-43 has a half-life of $T_{1/2}$ = 3.891 (12) h. It is a 100% β+ emitter and decays to Ca-43 (stable), by emitting a γ ray at 372.9 keV (see

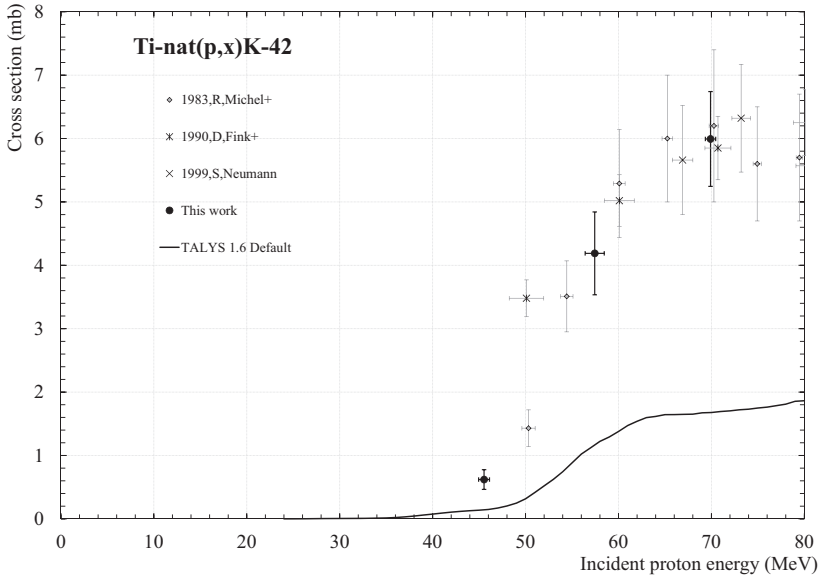

Fig. 7. Ti-nat(p,x) K-42 excitation function. (See above-mentioned references for further information.)

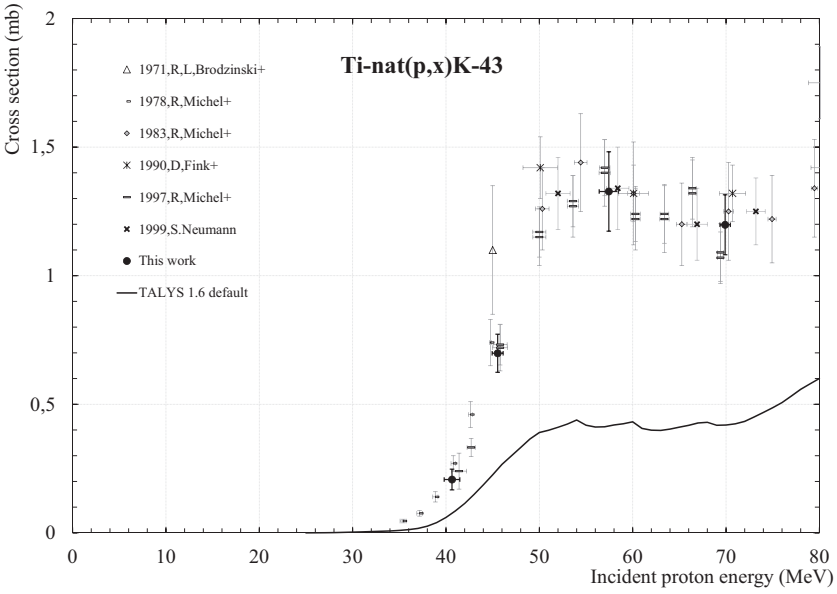

Fig. 8. Ti-nat(p,x) K-43 excitation function. (See above-mentioned references for further information.)

Table 2) with a branching ratio of 22.5%, used to deduce its activity. As there is some cooling time of about 14 h between the end of irradiation and the activity measurements, the short half-life of Sc-43 and its low production cross section have not allowed to detect and quantify Sc-43 in all the irradiated targets. When the Sc-43 activity in the target was high enough to be quantified by our experimental device, the estimated uncertainty on fit of the number of counts may be up to 20%. In addition, Sc-43 has only one detectable gamma line, common to K-43 which is also produced in the target above 30 MeV (see Table 2). The activity of K-43 was deduced from this peak using its others detectable gammas, resulting on an additional source of uncertainty for the determination of Sc-43 activity. Our results obtained above 30 MeV (see Fig. 1) give an order of magnitude of the Sc-43 cross section and further experiments are needed to complete its trend. The TALYS code (version 1.6 with default models) doesn't give satisfactory results for this reaction.

3.1.2. Production of Sc-44m

Sc-44m ($T_{1/2}$ = 58.6 (1) h) is of interest for medical applications as it can be used as in vivo generator [29,16] producing its ground state Sc-44g, useful for diagnostics. It can also be used in the Sc-44/Sc-47 theranostic pair [47]. It decays by Electron Capture (EC) process (1.20 (7)%) to Ca-44 (stable) by emitting three γ rays of 1001.83 (1.20%), 1126.06 (1.20%) and 1157.00 keV (1.20%). It mainly decays by Internal Transition (IT), at 98.80 (7)%, to its ground state Sc-44g ($T_{1/2}$ = 3.97 (4) h) by emitting an intense γ ray at 271.13 keV (Table 2). The high branching ratio of this last gamma line was used to extract the Sc-44m production cross section.

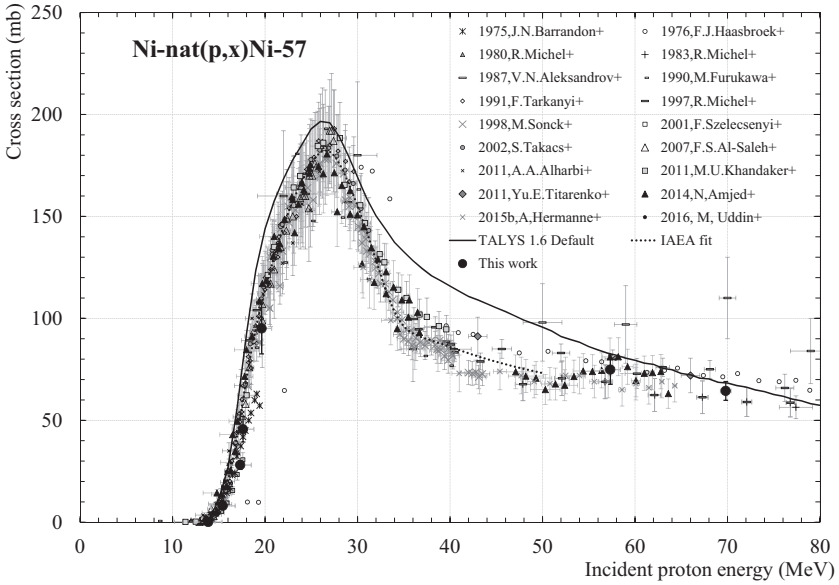

Fig. 9. Ni-nat(p,x) Ni-57 excitation function. (See above-mentioned references for further information.)

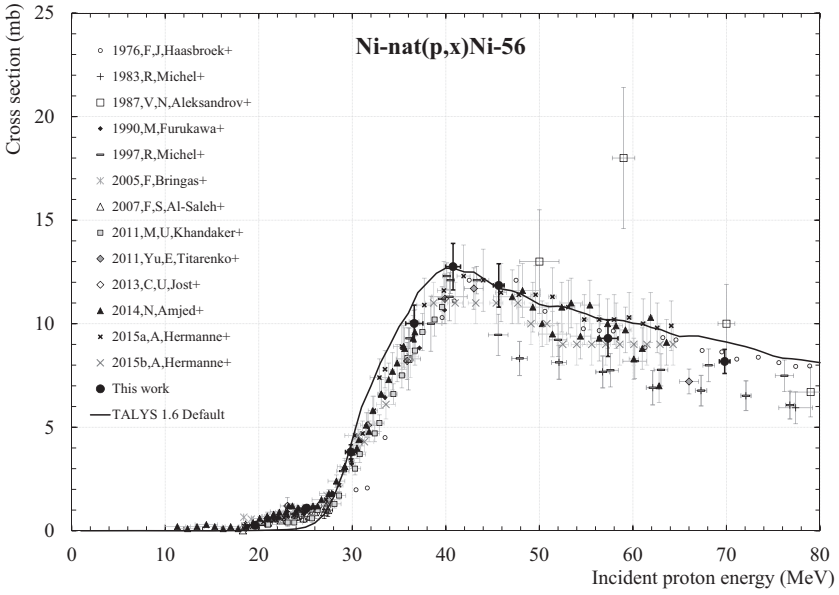

Fig. 10. Ni-nat(p,x) Ni-56 excitation function. (See above-mentioned references for further information.)

The results of the Ti-nat(p,x) Sc-44m excitation function are plotted in Fig. 2. Below 45 MeV, all the experimental values are in agreement, including the results of this work. Above this energy, our data are in agreement with Michel et al. [45] but further measurements are needed to better describe the curve. TALYS gives a good overall cross section estimate even if the amplitude of the peak at 32 MeV is underestimated. Looking at the amount of experimental results, Sc-44m should be considered for monitor reaction below 45 MeV. Sc-44m has a pretty long half-life (higher than 2 days) and an easily detectable gamma line for activity measurements.

3.1.3. Production of Sc-46

Sc-46 has a ground state Sc-46g and a metastable state Sc-46m. Sc-46m, with a very short half-life ($T_{1/2}$ = 18.75 (4) s), decays by IT (100%) to Sc-46g by emitting an intense γ ray of 142.528 keV. The half-life of Sc-46m is so short, that, at the time of our activity measurements, all the Sc-46m has decayed to Sc-46g ($T_{1/2}$ = 83.79 (4) days). We hence measured cumulative Sc-46m+g activities. Results relative to the Sc-46m+g cross section are plotted in Fig. 3.

The Ti-nat(p,x) Sc-46m+g reaction is considered by the IAEA as potential new monitor reaction [61] as Sc-46g has a long half-life and high cross section. Our data show a good agreement with all the general trend up to 45 MeV. From this energy, our data are close to the values of Michel et al. [45,48]. The recent values of Hermanne et al., [27] are 10% higher than our data but still agree within the error bars. TALYS 1.6 default gives very good results from 30 MeV.

3.1.4. Production of Sc-47

Sc-47 is particularly promising for $\beta-$ targeted therapy (Majkowska-Pilip and Bilewicz, 2011) and can be used for theranostic [47] with Sc-44. It has a half-life of 3.3492 (6) d and decays by $\beta-$ process at 100% to Ti-47 (stable) emitting an intense γ ray at

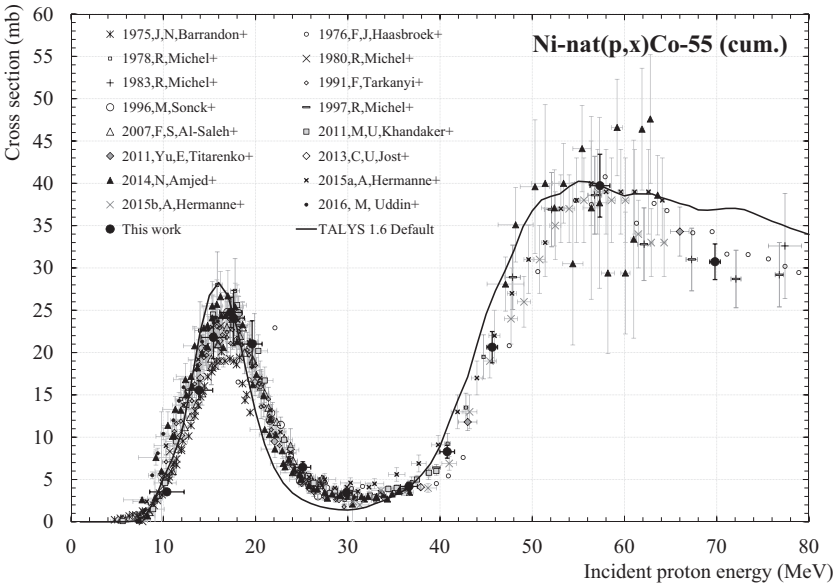

Fig. 11. Ni-nat(p,x) Co-55 (cum.) excitation function. (See above-mentioned references for further information.)

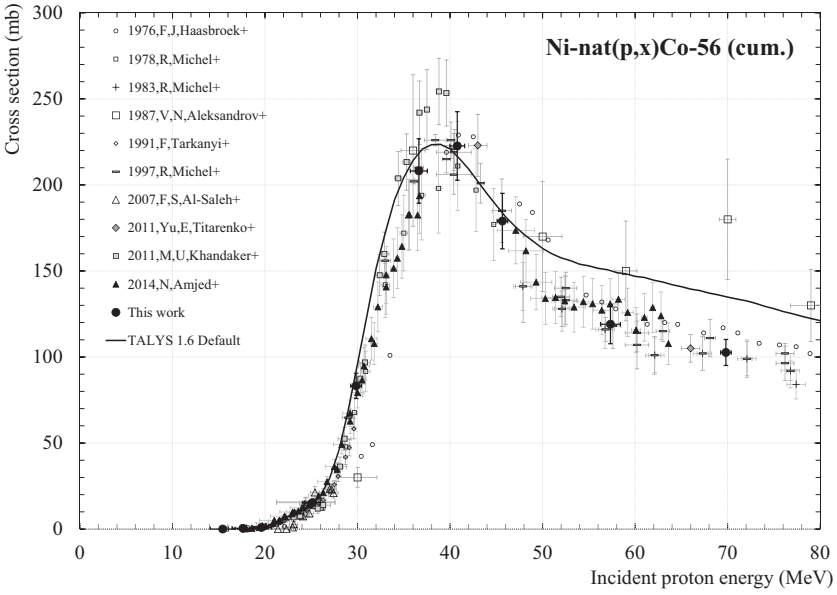

Fig. 12. Ni-nat(p,x) Co-56 (cum.) excitation function. (See above-mentioned references for further information.)

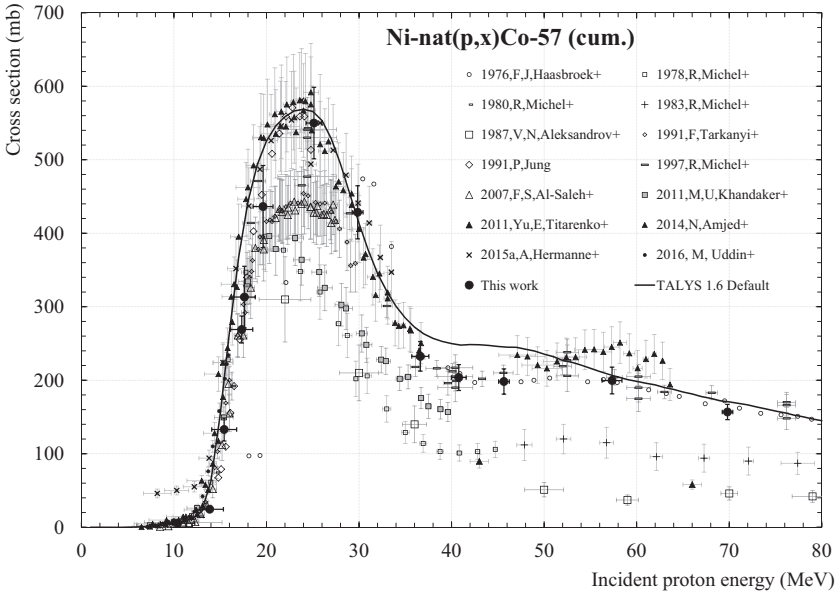

Fig. 13. Ni-nat(p,x) Co-57 (cum.) excitation function. (See above-mentioned references for further information.)

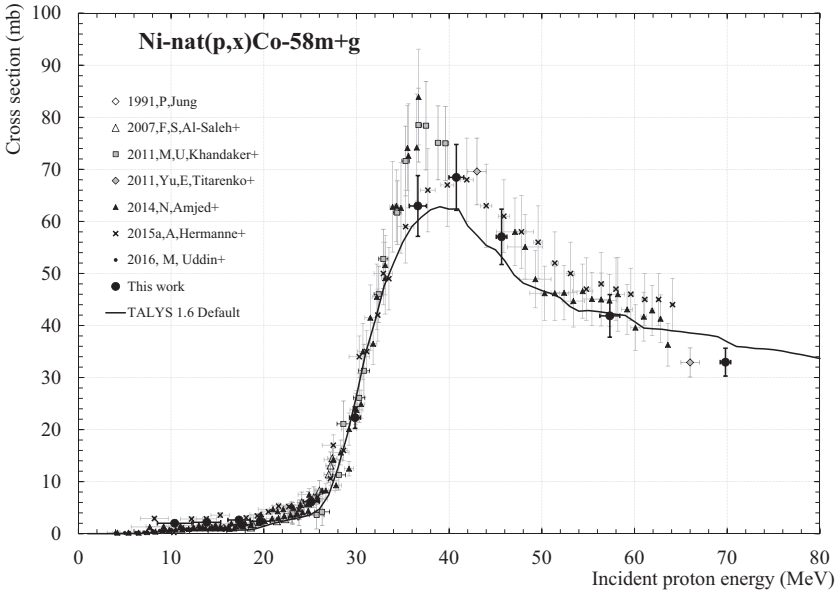

Fig. 14. Ni-nat(p,x) Co-58m+g excitation function. (See above-mentioned references for further information.)

159.377 keV (cf. Table 2). This γ line is used to derive the Sc-47 activity from the γ spectra. The Ti-nat(p,x) Sc-47 excitation function is plotted in Fig. 4.

Our data are in overall good agreement with the available experimental datasets, except with Brodzinski et al. [11], Michel et al. [44] and Fink et al. [18], that show higher values than the general behaviour. Further values are needed between 25 and 40 MeV to better assess the maximum of the cross section. TALYS (1.6 Default) is not able to reproduce the experimental values for this reaction.

3.1.5. Production of Sc-48

Sc-48, with a half-life of 43.67 (9) h, decays to Ti-48 (stable) by $\beta-$ emission (100%). It emits three γ lines with high branching ratio (higher than 97%) of 983.526, 1037.522 and 1312.120 keV, and a γ line with a lower intensity of 175.361 keV (7.48 (10)%). In Table 2, only two gamma lines are summarized which correspond to those used to determine Sc-48 activity. Only those two γ lines have been used as V-48 ($T_{1/2}$ = 15.9735 (25) d) is also produced in the titanium target and emits two γ lines at 983.526 and 1312.120 keV (see Table 2) that are common with Sc-48. The Sc-48 production cross section values are presented in Fig. 5.

Our data are in agreement with most of the published data. Data published in 1971 and 1983 give higher cross section values than the general behaviour, as already highlighted for the previous investigated scandium isotopes. The TALYS code overestimates the amplitude by 30% in comparison with our experimental values, but gives the good trend.

3.1.6. Production of V-48

V-48 is a 100% β+ emitter with a half-life of 15.9535 (25) days. It decays by emitting three main γ rays (see Table 2).

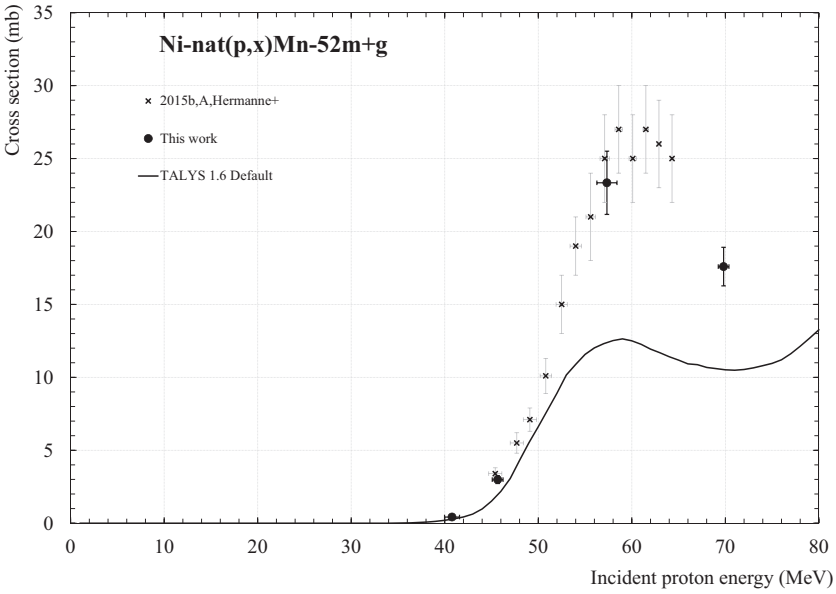

Fig. 15. Ni-nat(p,x) Mn-52m+g excitation function. (See above-mentioned references for further information.)

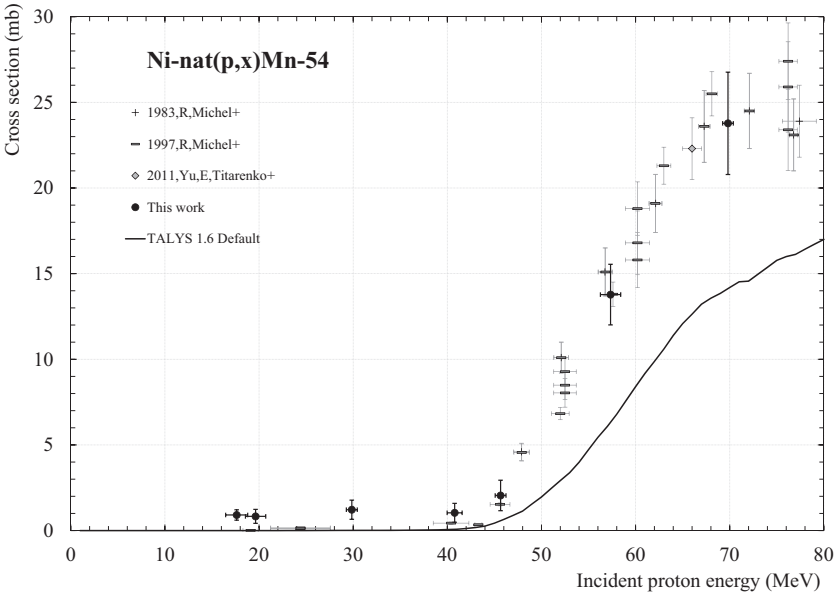

Fig. 16. Ni-nat(p,x) Mn-54 excitation function. (See above-mentioned references for further information.)

In each foil, the V-48 activity value has been determined after the complete decay of Sc-48 ($T_{1/2}$ = 43.67 h). Our new values (see Fig. 6), obtained above 20 MeV, are in agreement with the existing experimental data and with the recommended cross section values from the IAEA [59]. TALYS is able to reproduce this excitation function, even if the maximum is overestimated by 25%.

3.1.7. Production of K-42

K-42, with a half-life of 12.260 (3) hours, decays by $\beta-$ process (100%) to Ca-42 (stable). It emits a γ ray of 1524.7 keV with a branching ratio of 18%. This isotope can only be produced with protons with an energy higher than 40 MeV through (p,4p+xn) reactions (see Table 2).

Due to the high energy threshold (see Table 2), only three cross section values have been obtained in this work, plotted in Fig. 7. These data agree with the ones obtained by Michel et al. [44], Fink et al. [18] and Neumann, [48], within their error bars. Further experimental results are needed to have a complete dataset, especially below 60 MeV. TALYS doesn't reproduce the experimental trend.

3.1.8. Production of K-43

K-43 has a half-life of 22.3 (1) hours and decays by $\beta-$ emission at 100% to Ca-43 (stable), emitting four gamma rays with a branching ratio higher than 11% (see Table 2). Among these γ lines, one is common to Sc-43. Its contribution has been deduced to get K-43 activity. The three others γ lines have been also used to measure K-43 activity.

Our data obtained on the energy range 40–70 MeV are plotted in Fig. 8. They are in good agreement with the literature. Additional

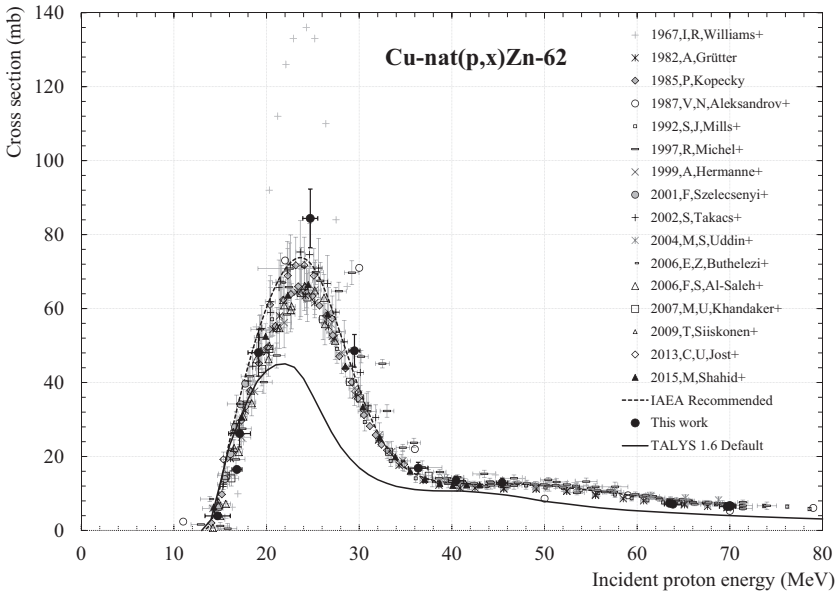

Fig. 17. Cu-nat(p,x) Zn-62 excitation function. (See above-mentioned references for further information.)

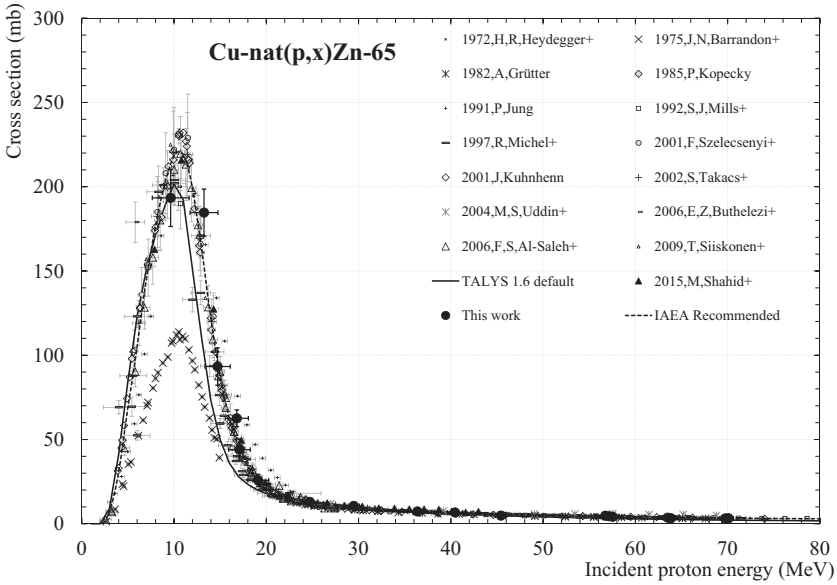

Fig. 18. Cu-nat(p,x) Zn-65 excitation function. (See above-mentioned references for further information.)

results are needed between 40 MeV and 50 MeV to refine the K-43 production cross section trend. TALYS is not able to reproduce the experimental cross section values.

3.2. Proton induced reactions on natural nickel

The Ni-nat(p,x) Ni-57 reaction is already defined as monitor reaction, with recommended cross section values evaluated by the IAEA. This reaction has been used to quantify the particle beam flux through our foils irradiated with protons between 20 MeV and 46 MeV. Our new results related to the production cross sections of nickel, cobalt and manganese isotopes in natural nickel are presented afterwards. Their physical characteristics are listed in Table 4 and their associated production cross section values are listed in Table 5.

3.2.1. Production of Ni-57

Ni-57 has a half-life of $T_{1/2}$ = 35.6 (6) h. It decays to Co-57 ($T_{1/2}$ = 271.79 (9) days) by EC/β+ emission process, emitting four principal γ rays, listed in Table 4, used to deduce its activity.

The amount of studies for the Ni-nat(p,x) Ni-57 reaction below 50 MeV allowed the International Atomic Energy Agency (IAEA) to set recommended cross section values for this reaction. Our data are plotted in Fig. 9. They were measured below 20 MeV and above 46 MeV. They are in good agreement with the existing experimental values and with the recommended cross section. TALYS 1.6

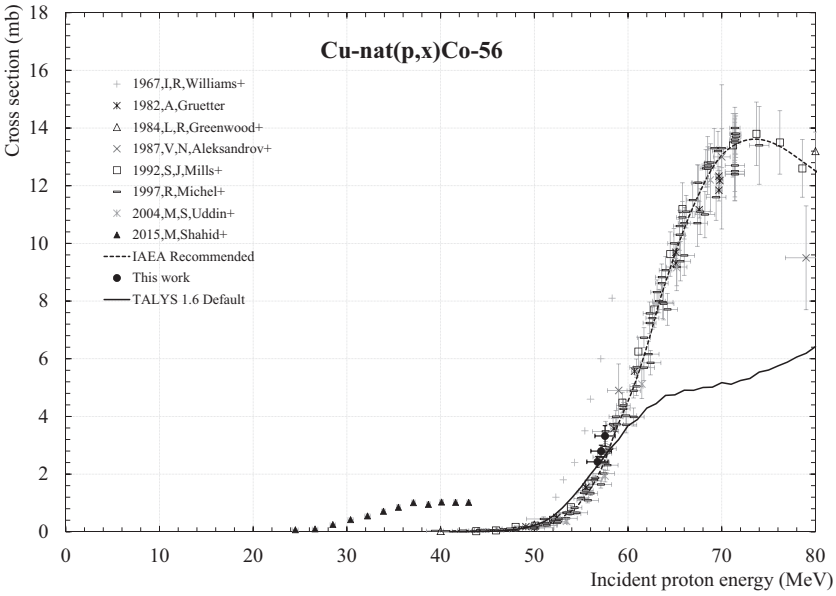

Fig. 19. Cu-nat(p,x) Co-56 excitation function. (See above-mentioned references for further information.)

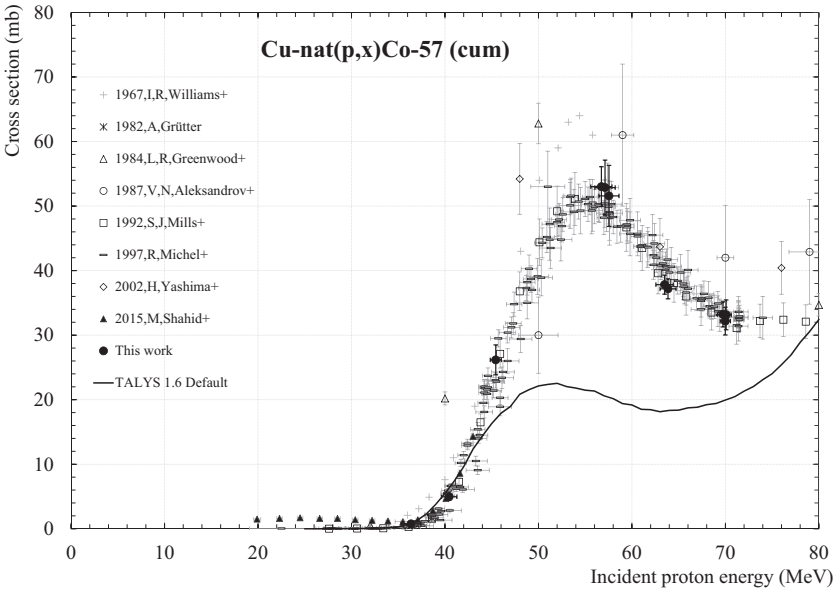

Fig. 20. Cu-nat(p,x) Co-57 (cum.) excitation function. (See above-mentioned references for further information.)

Default gives a good trend but overestimated in comparison with the experimental results.

3.2.2. Production of Ni-56

Ni-56, with a half-life of 6.077 (12) days, decays by EC/β+ emission to Co-56 ($T_{1/2}$ = 77.27 (3) days). The gamma lines used to determine Ni-56 activity are summarized in Table 4. The associated cross section values are plotted in Fig. 10.

Our data follow the general trend in the whole energy range. Above 40 MeV, the values of Michel et al. [45], are lower. The TALYS code gives good results above 40 MeV.

3.2.3. Cumulative production of Co-55

Co-55 is a CE/β+ emitter of interest for Position Emission Tomography [31,14], with a half-life of 17.53 (3) hours. It decays to Fe-55 (2.73 (3) years, no gamma emission). The gamma lines used to extract the Co-55 activity are listed in Table 4. With nickel as target, Ni-55 ($T_{1/2}$ = 209 ms) is produced via the Ni-58(p,p+3n) reaction above 39.8 MeV and decays to Co-55. Due to the very short half-life of Ni-55, our Co-55 production cross section results are then cumulative above 39.8 MeV.

Our data are in overall good agreement with all the existing data on the whole energy range. However, the data of Amjed et al. [4], are quite scattered. There is an energy shift between the TALYS results and the experimental data between 14 and 30 MeV, but it gives satisfactory results in overall.

3.2.4. Cumulative production of Co-56

Co-56 has a half-life of 77.27 (3) days and decays by CE/β+ process to Fe-56 (stable) by emitting 8 main γ rays, used to determine

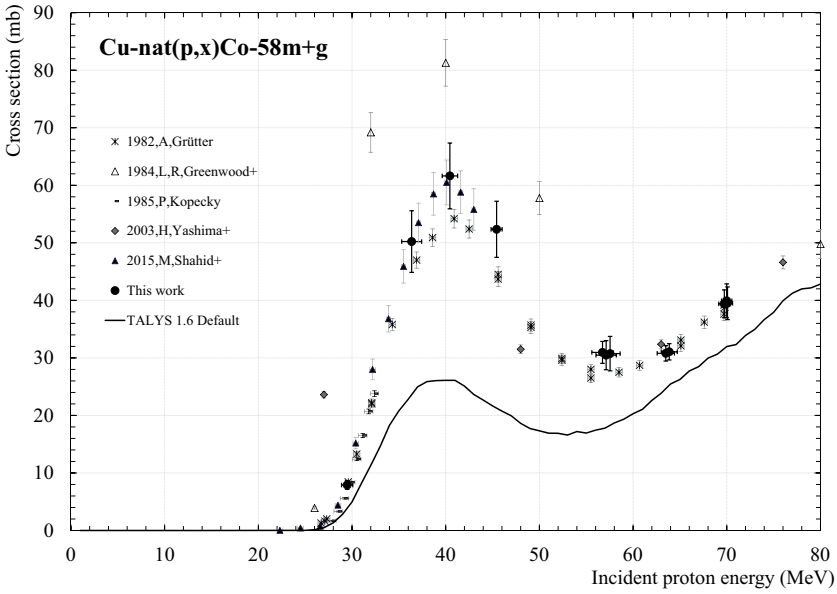

Fig. 21. Cu-nat(p,x) Co-58m+g excitation function. (See above-mentioned references for further information.)

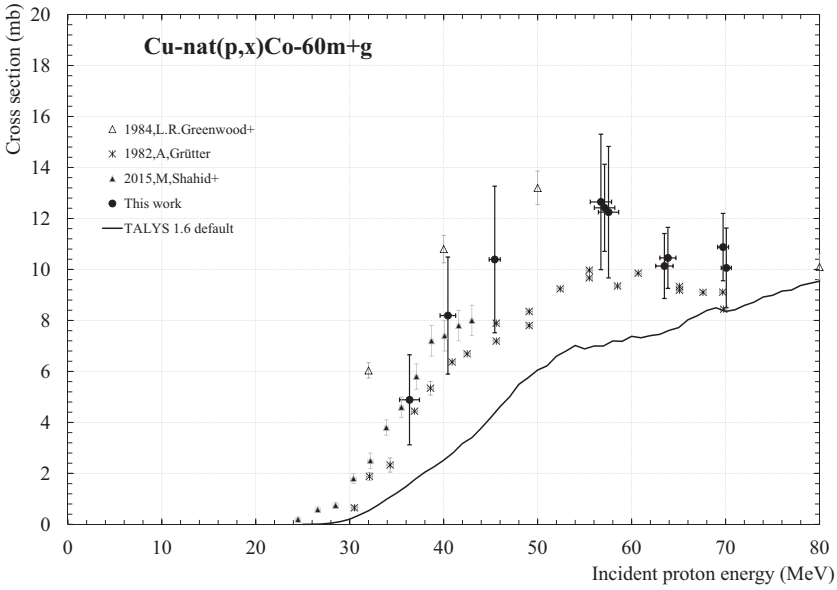

Fig. 22. Cu-nat(p,x) Co-60m+g excitation function. (See above-mentioned references for further information.)

the activity (see Table 4). Co-56 activity is obtained after the total decay of Ni-56 ($T_{1/2}$ = 6.077 (12) days), also produce in the nickel target, and which decays to Co-56 as specified in part 3.2.2. The Co-56 cross section values, presented in Fig. 12, are cumulative.

Our data are consistent with the exiting values on the whole energy range. However, the experimental values of Khandaker et al. [35], are higher between 35 and 45 MeV in comparison to our data and those of [44], are lower. This energy range contains the maximum of the Co-56 cumulative cross section and furthers experiments seems needed to refine it. The values of Aleksandrov et al. [2], are dispersed above 55 MeV, as highlighted with the Ni-56 production cross section. The TALYS code gives very satisfactory results up to 50 MeV.

3.2.5. Cumulative production of Co-57

Co-57 ($T_{1/2}$ = 271.79 (9) days) decays by EC process (100%) to Fe-57 (stable) by emitting ten γ rays, including two with a branching ratio higher than 10% and easily detectable (see Table 4). This radionuclide is fed by the decay of Ni-57, co-produced in the nickel target. Our Co-57 production cross section values are obtained after the complete decay of Ni-57 ($T_{1/2}$ = 35.6 (6) h).

The general trend gives a maximum around 550 mb. Our data are in agreement with this maximum and with the general trend. Some published data give lower values, that can be attributed to the incomplete decay of Ni-57 or to the measurement of independent Co-57 production cross section values. TALYS 1.6 default gives very good results.

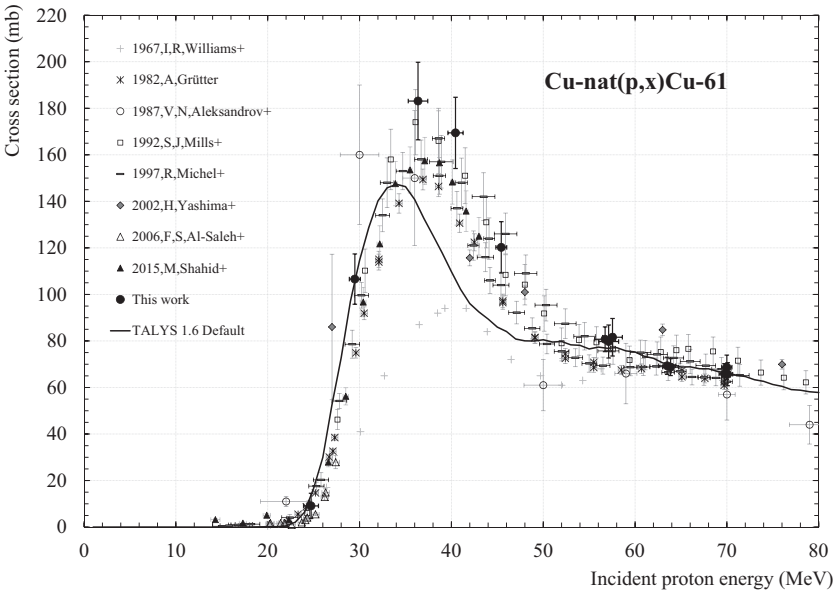

Fig. 23. Cu-nat(p,x) Cu-61 excitation function. (See above-mentioned references for further information.)

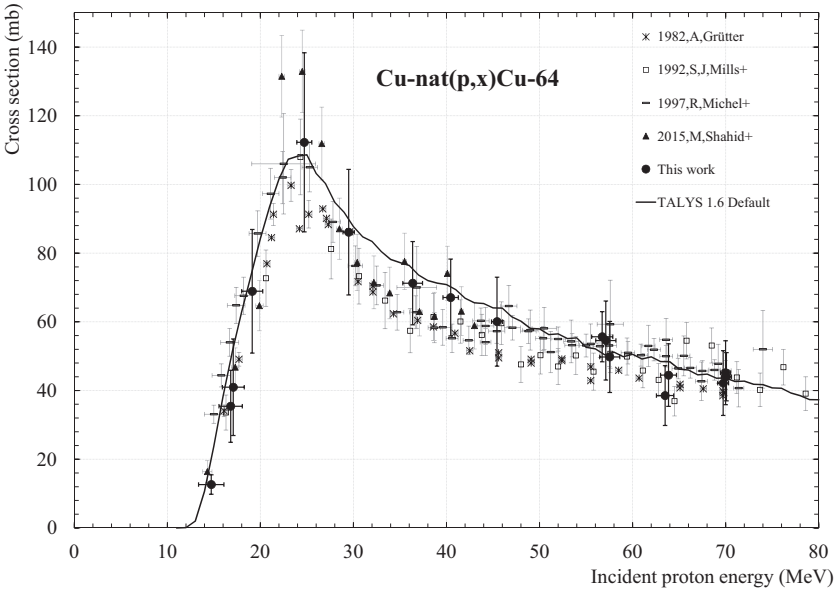

Fig. 24. Cu-nat(p,x) Cu-64 excitation function. (See above-mentioned references for further information.)

3.2.6. Production of Co-58m+g

Co-58 has a metastable state, Co-58m ($T_{1/2}$ = 9.04 (11) hours), which decays to its ground state, Co-58g, by emitting a low energy gamma ray (24.88 keV) with a branching ratio lower than 0.04%, not detectable in our experimental conditions. One detectable gamma ray with an energy of 811.775 keV (99%) is associated to the decay of Co-58g ($T_{1/2}$ = 70.86 (7) days). This γ line was used to determine its activity. The activity is measured one week after the end of irradiation, assuming that all Co-58m has decayed. The Co-58 cross section values, plotted in Fig. 14, include the metastable and the ground state production.

There is a good agreement between our values and the literature. However, the maximum value of the cross section around 38 MeV is different between the data sets of Khandaker et al. [35] and Amjed et al. [4], in comparison with this work and the values of Hermanne et al. [26]. The same difference with Khandaker et al. data has been already highlighted for Co-56 production cross section. For this isotope, other data are needed around the maximum of its cross section and above. The TALYS code gives good values whether in shape and amplitude.

3.2.7. Production of Mn-52m+g

Mn-52 has a metastable and a ground state, both promising for diagnostics [6,62]. The metastable state Mn-52m ($T_{1/2}$ = 21.1 (2) min) decays by IT (1.75%) to its ground state Mn-52g ($T_{1/2}$ = 5.591 (3) days) and by β+ emission (98.25%) to Cr-52 (stable). The ground state Mn-52g decays at 100% by CE/β+ to Cr-52 (stable). Due to its short half-life, this metastable state decayed between the end of irradiation and the activity measurements. This way, we were only able to measure the cumulative

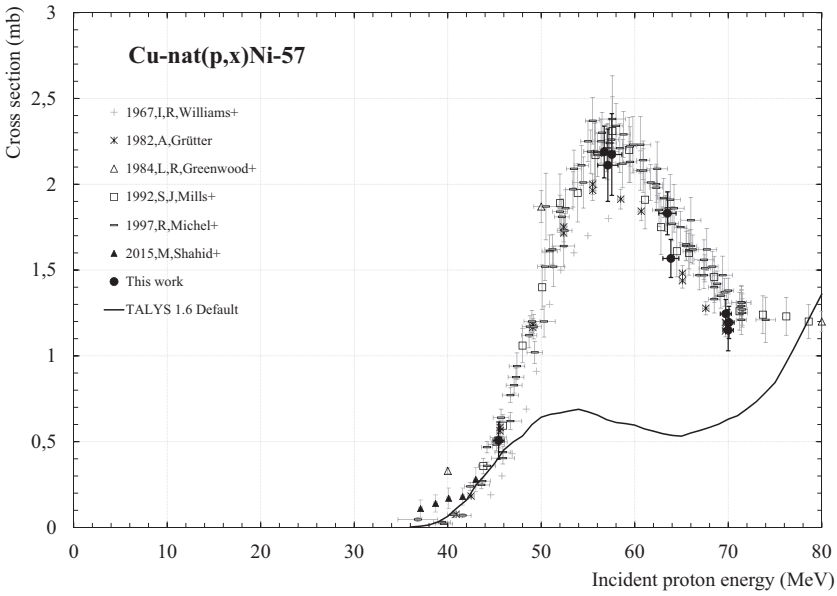

Fig. 25. Cu-nat(p,x) Ni-57 excitation function. (See above-mentioned references for further information.)

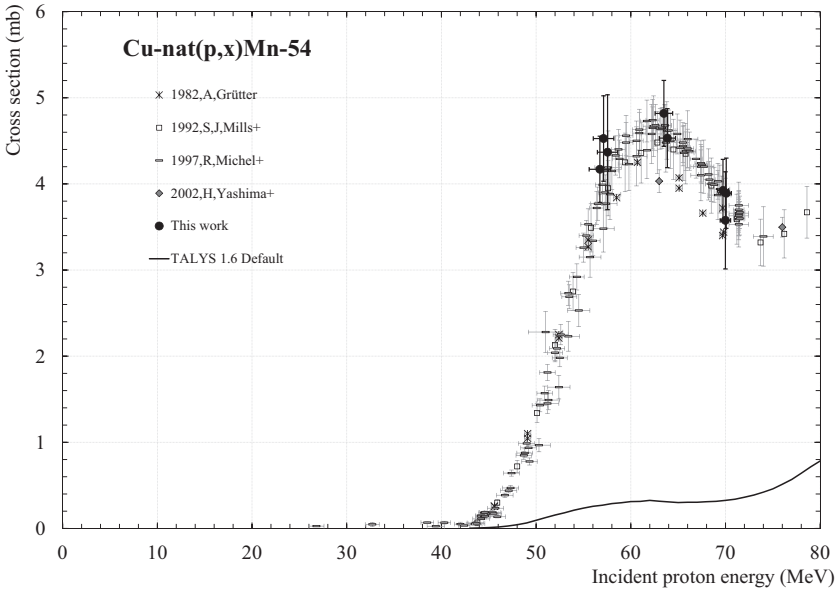

Fig. 26. Cu-nat(p,x) Mn-54 excitation function. (See above-mentioned references for further information.)

activity coming from the direct production of Mn-52g and the decay of Mn-52m. The related cross section results are plotted in Fig. 15.

The Mn-52m+g cross section results show a maximum around 55 MeV. Our data are in agreement with Hermanne et al. [26,28]. Further measurements are needed to better refine the trend, above 65 MeV. The TALYS code gives the good shape but underestimates by 50% from 50 MeV.

3.2.8. Production of Mn-54

Mn-54 has a long half-life (312.3 (4) days). It decays by CE process (100%) to Cr-54 (stable), emitting one gamma ray (see Table 4), used to extract Mn-54 activity.

Our results follow those previously published by Michel et al. [44], Michel et al. [45] and Titarenko et al. [60]. Once again, TALYS gives the good trend but underestimates the experimental results.

3.3. Proton induced reactions on natural copper

The IAEA has defined recommended cross section values for the Cu-nat(p,x) Zn-62,65, Co-56 reactions and proposes the Cu-nat(p,x) Co-58 as potential additional monitor reaction [61]. In this study, the Cu-nat(p,x) Zn-62 reaction has been used as monitor between 46 MeV and 60 MeV, and the Cu-nat(p,x) Co-56 reaction has been used as monitor reaction above 60 MeV. The physical characteristics of the radionuclides produced in the copper foils are listed in Table 6 and their associated production cross section values are presented in Table 7.

3.3.1. Production of Zn-62

Zn-62 is of medical interest as it produces, by decay, the PET imaging agent Cu-62 [50]. In addition, the Cu-nat(p,x) Zn-62 reaction is defined as monitor reaction with recommended values

Table 3
Experimental cross section values for Ti-nat(p,x) Sc-43,44m,46,47,48, V-48, K-42,43 reactions.

Energy (MeV)	σ Sc-43 (mb)	σ Sc-44m (mb)	σ Sc-46 (mb)	σ Sc-47 (mb)
69.90 ± 0.56	8.81 ± 2.76	18.74 ± 1.29	45.07 ± 3.14	19.39 ± 1.31
57.44 ± 1.03	11.85 ± 4.33	12.43 ± 1.17	51.21 ± 4.87	20.35 ± 1.89
45.54 ± 0.59	11.84 ± 4.83	10.78 ± 0.96	63.98 ± 5.85	19.17 ± 1.69
40.64 ± 0.84		12.88 ± 1.15	60.15 ± 5.52	20.59 ± 1.81
36.48 ± 0.91		15.46 ± 1.37	43.21 ± 3.93	22.43 ± 1.96
29.65 ± 0.59		15.38 ± 1.36	14.53 ± 1.37	24.44 ± 2.11
24.90 ± 0.80		8.33 ± 0.78	10.42 ± 1.01	15.21 ± 1.38
19.36 ± 1.09		1.07 ± 0.17	5.18 ± 0.76	4.26 ± 0.56
17.33 ± 1.16		1.00 ± 0.16	3.94 ± 0.62	1.84 ± 0.27
17.06 ± 1.26		0.97 ± 0.07	3.45 ± 0.51	1.37 ± 0.14
15.11 ± 1.34	3.47 ± 2.08	0.75 ± 0.09	2.80 ± 0.40	0.88 ± 0.10
13.55 ± 1.48		0.53 ± 0.22		0.72 ± 0.16
10.01 ± 1.90				
Energy (MeV)	σ Sc-48 (mb)	σ V-48 (mb)	σ K-42 (mb)	σ K-43 (mb)
69.90 ± 0.56	1.81 ± 0.17	10.37 ± 0.73	5.99 ± 0.75	1.20 ± 0.12
57.44 ± 1.03	1.83 ± 0.22	14.48 ± 1.48	4.19 ± 0.65	1.33 ± 0.15
45.54 ± 0.59	1.53 ± 0.15	19.24 ± 1.84	0.62 ± 0.16	0.70 ± 0.07
40.64 ± 0.84	1.40 ± 0.14	25.25 ± 2.37		0.21 ± 0.04
36.48 ± 0.91	1.11 ± 0.12	29.03 ± 2.65		
29.65 ± 0.59	0.65 ± 0.14	36.93 ± 3.39		
24.90 ± 0.80	0.34 ± 0.12	51.26 ± 4.79		
19.36 ± 1.09				
17.33 ± 1.16				
17.06 ± 1.26				
15.11 ± 1.34				
13.55 ± 1.48				
10.01 ± 1.90				

defined by the IAEA [59]. Zn-62 has a half-life of 9.1786 (13) hours and decays by EC/β+ process (100%) to Cu-62 ($T_{1/2}$ = 9.74 (2) min), by emitting different detectable γ lines (see Table 6). New data have been obtained (see Fig. 17) for Zn-62 production cross section using the Ti-nat(p,x) V-48, Ni-nat(p,x) Ni-57 and Cu-nat(p,x) Co-56 monitor reactions.

Our values are in overall good agreement with the literature and follow the recommended cross section, except our maximum that is 10% to 20% higher depending on the dataset used for comparison. Due to the spread between the dataset for the quantification of this maximum, further values have to be obtained to better estimate it. TALYS 1.6 Default results give the good trend but underestimate the cross section amplitude.

3.3.2. Production of Zn-65

Zn-65 ($T_{1/2}$ = 244.26 (26) days) decays by EC/β+ process (100%) to Cu-65 (stable) by emitting three γ rays. Among these γ lines, the one at 1115.546 keV (50.60 (24)%) was detectable by our device in our experimental conditions. Our new cross section results are plotted in Fig. 18.

Our data points are in agreement with the literature and the recommended cross section. Between 8 and 18 MeV, TALYS values are too low compared to the experimental ones.

3.3.3. Production of Co-56

The physical characteristics of Co-56 have been presented in part 3.2.4, and are listed in Table 6. It is considered as independent because no Ni-56 has been detected in the copper targets. The Cu-nat(p,x) Co-56 reaction has a recommended cross section defined by the IAEA committee members.

Three data points have been obtained in this work between 56 and 58 MeV, using Zn-62 as monitor. Our data are plotted in Fig. 19, with data from the literature. They follow the recommended values. Data from Shahid et al. (2016) are in strong disagreement with the other ones, due to recoil activity coming from the nickel foils, which were placed before the copper foils. No additional data seems needed in the 40–70 MeV energy range for this reaction. However, TALYS 1.6 Default is not able to reproduce this excitation function but gives the good trend.

3.3.4. Cumulative production of Co-57

The physical characteristics of Co-57 have been presented in part 3.2.5, and are listed in Table 6. The production cross section values are obtained after the total decay of Ni-57 co-produced in the target (see part 3.3.3).

Our data, plotted in Fig. 20, follow the trend of Grütter, [22], Mills et al. [46], Michel et al. [45] and Yashima et al. [67]. Data published in William and Fulmer, William and Fulmer [65], Greenwood and Smither, [21] and Aleksandrov et al. [2] are not in agreement with the general behaviour. As for Co-56, the values published by Shahid et al. [53], are contaminated by the Co-57 recoil nuclei produced in the nickel foils. TALYS results do not agree with the experimental ones.

3.3.5. Production of Co-58m+g

The physical characteristics of Co-58 have been presented in part 3.2.6, and are listed in Table 6. Our cumulative production cross section values for Co-58m+g production in copper are presented in Table 5 and plotted in Fig. 21.

Our points are in good agreement with the work published by Grütter, [22], Kopecky, [38] and Shahid et al. [53], but not with Greenwood and Smither, [21] and Yashima et al. [67] below 55 MeV. The maximum of the cross section, reproduces by our points around 40 MeV, is in agreement with the values of Grütter, [22] and Shahid et al. [53]. However, we have to take into account some Co-58 recoil nuclei in the experiment of Shahid et al. [53]. The maximum plotted by the data of Greenwood and Smither, [21], are 20% higher than our value. The TALYS code gives the good trend but underestimates the amplitude of the cross section in comparison with the experimental values.

3.3.6. Production of Co-60m+g

The metastable state Co-60m, with a half-life of 10.467 (6) min, decays by IT process (99.76%) to its ground state Co-60g and by $\beta-$ emission (0.24%) to Ni-60 (stable). Co-60g has a long half-life of 5.2714 (5) years and is a 100% $\beta-$ emitter. Due to the short half-life of Co-60m, we were only able to determine the cumulative activity of both states: Co-60m+g. The related cross section values are plotted in Fig. 22.

Only 4 to 15 Bq of Co-60 were measured in our targets, in our experimental conditions. The values obtained by [21], are also cumulative and expressed with 5% of uncertainty. Our data are compatible with the experiment of Shahid et al. [53]. No uncertainty is specified on Grütter, [22] values. TALYS gives a quite good trend but underestimated.

3.3.7. Production of Cu-61

Cu-61 is among the list of copper isotopes well suitable for PET imaging [66]. Cu-61 has a half-life of 3.333 (5) hours and decays by EC/β+ process to Ni-61 (stable). The gamma lines used to determine the Cu-61 activity are listed in Table 6. The production cross section values are presented in Table 5 and plotted in Fig. 23.

Our data follow the general trend. Our values are especially in agreement with Mills et al. [46] in the whole energy range. Our data are also in good agreement with Michel et al. [45] and Grütter, [22], within the error bars. TALYS gives good results except in the 35–50 MeV energy range, where the values are too low in comparison with the experimental results.

Table 4
Physical characteristics of the radionuclides produced in nickel [36,17] and reaction thresholds [51].

Radioisotope	$T_{1/2}$	E_γ (keV)	I_γ (%)	Contributing reactions	Threshold (MeV)
Ni-56	6.077 (12) d	158.38	98.8 (10)	Ni-58(p,p+2n)	22.85
		269.5	36.5 (8)	Ni-60(p,p+4n)	43.57
		480.44	36.5 (8)	Ni-61(p,p+5n)	51.51
		749.95	49.5 (12)	Ni-62(p,p+6n)	62.26
		811.85	86.0 (9)		
		1561.8	14.0 (6)		
Ni-57	35.60 (6) h	127.164	16.7 (3)	Ni-58(p,p+n)	12.43
		1377.64	81.7 (16)	Ni-60(p,p+3n)	33.15
		1757.55	5.75 (16)	Ni-61(p,p+4n)	41.09
		1919.52	12.26 (25)	Ni-62(p,p+5n)	51.85
				Ni-64(p,p+7n)	68.58
Co-55	17.53 (3) h	91.9	1.16 (7)	Ni-58(p,α)	1.36
		411.9	1.07 (7)	Ni-58(p,2p+2n)	30.15
		477.2	20.2 (14)	Ni-60(p,α+2n)	22.09
		803.4	1.87 (13)	Ni-60(p,2p+4n)	50.86
		931.3	75	Ni-61(p,α+3n)	30.03
		1316.4	7.09 (10)	Ni-61(p,2p+5n)	65.19
		1369.7	2.92 (22)	Ni-62(p,α+4n)	40.79
		1408.4	16.88 (8)	Ni-64(p,α+6n)	57.53
Co-56	77.27 (3) d	846.771	100	Ni-58(p,d+p)	17.63
		1037.84	13.99 (10)	Ni-58(p,2p+n)	19.89
		1238.282	67.6 (4)	Ni-60(p,α+n)	11.84
		1360.215	4.33 (4)	Ni-60(p,He-3+2n)	32.76
		1771.351	15.69 (15)	Ni-60(p,2p+3n)	40.61
				Ni-61(p,α+2n)	19.78
				Ni-61(p,He-3+3n)	40.70
				Ni-61(p,2p+4n)	48.55
				Ni-62(p,α+3n)	30.54
				Ni-62(p,He-3+4n)	51.46
				Ni-62(p,2p+5n)	59.30
				Ni-64(p,α+5n)	47.28
				+ Ni-56 decay	
Co-57	271.79 (9) d	122.0614	85.60 (17)	Ni-58(p,2p)	8.31
		136.4743	10.68 (8)	Ni-60(p,α)	0.27
				Ni-60(p,He-3+n)	21.19
				Ni-60(p,2p+2n)	29.04
				Ni-61(p,α+n)	8.22
				Ni-61(p,He-3+2n)	29.14
				Ni-61(p,2p+3n)	36.98
				Ni-62(p,α+2n)	18.98
				Ni-62(p,He-3+3n)	39.90
				Ni-62(p,2p+4n)	47.74
				Ni-64(p,α+4n)	35.73
				Ni-64(p,He-3+5n)	56.63
				Ni-64(p,2p+6n)	64.47
				+ Ni-57 decay	
Co-58	70.86 (7) d	810.775	99	Ni-60(p,d+p)	18.06
				Ni-60(p,2p+n)	20.32
				Ni-61(p,α)	0.00
				Ni-61(p,He-3+n)	20.42
				Ni-61(p,2p+2n)	28.27
				Ni-62(p,α+n)	10.27
				Ni-62(p,He-3+2n)	31.18
				Ni-62(p,2p+3n)	39.03
				Ni-64(p,α+2n)	18.98
				Ni-64(p,He-3+2n)	39.90
				Ni-64(p,2p+3n)	47.74
Mn-52	5.591 (3) d	744.233	90.0 (8)	Ni-58(p,α+2p+n)	27.78
		935.538	94.5 (9)	Ni-58(p,He-3+2p+2n)	48.72
		1246.278	4.21 (6)	Ni-60(p,2α+n)	19.72
		1333.649	5.07 (5)	Ni-60(p,α+2p+3n)	48.50
		1434.068	100.0 (5)	Ni-61(p,2α+2n)	27.67
				Ni-61(p,α+2p+4n)	56.43
				Ni-62(p,2α+3n)	38.43
				Ni-62(p,α+2p+5n)	67.19
Mn-54	312.3 (4) d	834.848	99.976 (1)	Ni-58(p,4p+n)	35.21
				Ni-60(p,α+2p+n)	27.15
				Ni-60(p,He-3+2p+2n)	48.07
				Ni-60(p,4p+3n)	55.92
				Ni-61(p,2α)	6.33
				Ni-61(p,4p+4n)	63.86
				Ni-62(p,2α+n)	17.10
				Ni-64(p,2α+3n)	33.84

Table 5
Experimental cross section values for Ni-nat(p,x) Co-55,56,57,58, Ni-56,57, Mn-52,54 reactions.

Energy (MeV)	σ Co-55 (mb)	σ Co-56 (mb)	σ Co-57 (mb)	σ Co-58 (mb)
69.81 ± 0.57	30.73 ± 2.11	102.63 ± 7.56	156.77 ± 10.42	32.95 ± 2.68
57.34 ± 1.07	39.72 ± 3.71	119.03 ± 11.32	199.61 ± 18.18	41.85 ± 4.09
45.66 ± 0.58	20.64 ± 1.85	178.99 ± 16.14	198.22 ± 17.17	57.04 ± 5.32
40.78 ± 0.80	8.28 ± 0.76	222.65 ± 19.93	203.67 ± 17.60	68.46 ± 6.33
36.63 ± 0.92	4.18 ± 0.40	208.11 ± 18.74	232.48 ± 20.11	62.97 ± 5.84
29.85 ± 0.58	3.43 ± 0.38	83.22 ± 7.36	428.46 ± 36.16	22.30 ± 2.05
25.13 ± 0.85	6.45 ± 0.65	15.36 ± 1.49	549.91 ± 48.68	6.15 ± 0.64
19.63 ± 1.08	21.01 ± 2.75	0.96 ± 0.17	436.30 ± 55.85	2.40 ± 0.35
17.62 ± 1.17	24.08 ± 3.28	0.43 ± 0.10	313.11 ± 41.96	1.70 ± 0.26
17.33 ± 1.20	24.75 ± 1.79		268.99 ± 18.39	2.63 ± 0.21
15.43 ± 1.35	21.79 ± 2.50		132.96 ± 15.68	
13.86 ± 1.49	15.55 ± 1.13		24.42 ± 1.72	2.20 ± 0.23
10.39 ± 1.86	3.54 ± 0.33		5.45 ± 0.59	2.00 ± 0.25
Energy (MeV)	σ Ni-56 (mb)	σ Ni-57 (mb)	σ Mn-52 (mb)	σ Mn-54 (mb)
69.81 ± 0.57	8.18 ± 0.58	64.41± 4.62	17.59 ± 1.32	23.78 ± 2.99
57.34 ± 1.07	9.29 ± 0.88	74.85 ± 7.19	23.34 ± 2.17	13.78 ± 1.77
45.66 ± 0.58	11.85 ± 1.05		2.99 ± 0.27	2.05 ± 0.89
40.78 ± 0.80	12.75 ± 1.13		0.42 ± 0.05	1.04 ± 0.55
36.63 ± 0.92	10.01 ± 0.89			
29.85 ± 0.58	3.80 ± 0.35			1.22 ± 0.56
25.13 ± 0.85	1.10 ± 0.13			
19.63 ± 1.08	0.26 ± 0.07	95.08 ± 12.52		0.83 ± 0.41
17.62 ± 1.17		45.63 ± 6.27		0.91 ± 0.30
17.33 ± 1.20		28.07 ± 2.12		
15.43 ± 1.35		8.07 ± 0.96		
13.86 ± 1.49		0.13 ± 0.04		
10.39 ± 1.86				

Table 6
Physical characteristics of the radionuclides produced in copper [36,17] and reaction thresholds [51].

Radioisotope	$T_{1/2}$	E_γ (keV)	I_γ (%)	Contributing reactions	Threshold (MeV)
Zn-62	9.1786 (13) h	243.39	2.52 (13)	Cu-63(p,2n)	13.48
		246.96	1.9 (1)	Cu-65(p,4n)	31.57
		260.43	1.35 (8)		
		394.03	2.236 (10)		
		548.35	15.3 (8)		
		596.56	26		
Zn-65	244.26 (26) d	1115.546	50.60 (24)	Cu-65(p,n)	2.17
Ni-57	35.60 (6) h	127.164	16.7 (3)	Cu-63(p,α+3n)	29.31
		1377.64	81.7 (16)	Cu-63(p,He-3+4n)	50.21
		1757.55	5.75 (16)	Cu-63(p,2p+5n)	58.06
		1919.52	12.26 (25)	Cu-65(p,α+5n)	47.40
				Cu-65(p,He-3+6n)	68.29
Co-56	77.27 (3) d	846.771	100	Cu-63(p,α+p+3n)	36.76
		1037.84	13.99 (10)	Cu-63(p,3p+5n)	65.51
		1238.282	67.6 (4)	Cu-65(p,α+p+5n)	54.84
		1360.215	4.33 (4)		
		1771.351	15.69 (15)		
Co-57	271.79 (9) d	122.0614	85.60 (17)	Cu-63(p,α+p+2n)	25.20
		136.4743	10.68 (8)	Cu-63(p,He-3+p+3n)	46.11
				Cu-63(p,3p+4n)	53.95
				Cu-65(p,α+p+4n)	47.00
				Cu-65(p,He-3+p+5n)	64.19
				+ Ni-57 decay	
Co-58	70.86 (7) d	810.775	99	Cu-63(p,α+p+n)	16.49
				Cu-63(p,He-3+p+2n)	37.40
				Cu-63(p,3p+3n)	45.24
				Cu-65(p,α+p+3n)	34.58
				Cu-65(p,He-3+p+4n)	55.48
				Cu-65(p,3p+5n)	63.32
Co-60	5.2714 (5) y	1173.237	99.9736 (7)	Cu-63(p,3p+n)	27.00
		1332.501	99.9856 (4)	Cu-65(p,α+p+n)	16.36
				Cu-65(p,3p+3n)	45.09
Cu-61	3.333 (5) h	282.956	12.2 (3)	Cu-63(p,p+2n)	20.05
		373.05	2.15 (5)	Cu-65(p,p+4n)	38.15
		588.605	1.168 (21)		
		656.008	10.77 (18)		
		908.631	1.102 (21)		
		1185.234	3.75 (7)		

Table 6 (*continued*)

Radioisotope	$T_{1/2}$	E_γ (keV)	I_γ (%)	Contributing reactions	Threshold (MeV)
Cu-64	12.700 (2) h	1345.84	0.473 (10)	Cu-65(p,d)	7.81
				Cu-65(p,p+n)	10.06
Mn-54	312.3 (4) d	834.848	99.976 (1)	Cu-63(p,2α+d)	21.05
				Cu-63(p,2α+p+n)	23.31
				Cu-65(p,2α+d+2n)	39.14
				Cu-65(p,2α+p+3n)	41.40

Table 7
Experimental cross section values for Cu-nat(p,x) Zn-62,65, Ni-57, Co-56,57,58,60, Cu-61,64, Mn-54 reactions.

Energy (MeV)	σ Zn-62 (mb)	σ Zn-65 (mb)	σ Ni-57 (mb)	σ Co-56 (mb)
70.08 ± 0.54	6.59 ± 0.51	3.28 ± 0.54	1.19 ± 0.09	
69.99 ± 0.55	6.71 ± 0.53	2.89 ± 0.80	1.15 ± 0.12	
69.73 ± 0.59	6.46 ± 0.43	3.17 ± 0.48	1.24 ± 0.08	
63.86 ± 0.86	7.11 ± 0.38	3.28 ± 0.42	1.57 ± 0.11	
63.49 ± 0.92	7.34 ± 0.39	3.62 ± 0.48	1.83 ± 0.12	
57.55 ± 1.07		4.17 ± 0.90	2.17 ± 0.24	3.32 ± 0.36
57.12 ± 1.09		4.46 ± 0.62	2.11 ± 0.21	2.80 ± 0.20
56.74 ± 1.13		4.81 ± 0.56	2.12 ± 0.15	2.43 ± 0.19
45.43 ± 0.59	12.89 ± 1.23	4.82 ± 1.16	0.51 ± 0.11	
40.45 ± 0.83	13.45 ± 1.26	6.73 ± 1.03		
36.37 ± 1.06	16.84 ± 1.58	7.31 ± 0.94		
29.48 ± 0.60	48.57 ± 4.42	10.62 ± 1.45		
24.72 ± 0.81	84.37 ± 7.93	12.98 ± 1.85		
19.13 ± 1.13	48.07 ± 6.35	25.74 ± 3.58		
17.09 ± 1.18	26.20 ± 3.63	43.97 ± 6.29		
16.81 ± 1.25	16.49 ± 1.29	62.58 ± 4.99		
14.72 ± 1.37	3.94 ± 0.47	93.30 ± 11.09		
13.25 ± 1.51		184.64 ± 14.00		
9.64 ± 1.99		193.38 ± 16.97		
Energy (MeV)	σ Co-57 (mb)	σ Co-58 (mb)	σ Co-60 (mb)	σ Mn-54 (mb)
70.08 ± 0.54	33.15 ± 2.31	39.50 ± 2.84	10.06 ± 1.56	3.89 ± 0.41
69.99 ± 0.55	32.18 ± 2.15	39.92 ± 2.94		3.58 ± 0.56
69.73 ± 0.59	33.21 ± 1.94	39.40 ± 2.42	10.88 ± 1.32	3.92 ± 0.36
63.86 ± 0.86	37.17 ± 1.55	31.05 ± 1.41	10.45 ± 1.20	4.53 ± 0.34
63.49 ± 0.92	37.83 ± 1.48	30.79 ± 1.34	10.13 ± 1.27	4.82 ± 0.38
57.55 ± 1.07	51.58 ± 4.73	30.74 ± 3.00	12.25 ± 2.58	4.37 ± 0.67
57.12 ± 1.09	52.86 ± 4.26	30.47 ± 2.52	12.42 ± 1.71	4.53 ± 0.50
56.74 ± 1.13	53.01 ± 3.09	30.95 ± 1.91	12.65 ± 2.66	4.17 ± 0.38
45.43 ± 0.59	26.17 ± 2.32	52.34 ± 4.88	10.39 ± 2.88	
40.45 ± 0.83	4.96 ± 0.52	61.63 ± 5.72	8.19 ± 2.30	
36.37 ± 1.06	0.76 ± 0.22	50.22 ± 5.35	4.89 ± 1.77	
29.48 ± 0.60		7.90 ± 0.76		
24.72 ± 0.81				
19.13 ± 1.13				
17.09 ± 1.18				
16.81 ± 1.25				
14.72 ± 1.37				
13.25 ± 1.51				
9.64 ± 1.99				
Energy (MeV)	σ Cu-61 (mb)	σ Cu-64 (mb)		
70.08 ± 0.54	65.72 ± 4.96	44.02 ± 7.03		
69.99 ± 0.55	68.72 ± 5.20	45.18 ± 9.32		
69.73 ± 0.59	65.85 ± 4.39	42.16 ± 9.42		
63.86 ± 0.86	68.75 ± 3.63	44.49 ± 9.12		
63.49 ± 0.92	69.31 ± 3.70	38.54 ± 8.71		
57.55 ± 1.07	81.59 ± 8.08	49.78 ± 10.34		
57.12 ± 1.09	79.75 ± 7.09	54.57 ± 11.50		
56.74 ± 1.13	80.73 ± 5.32	55.66 ± 7.31		
45.43 ± 0.59	120.22 ± 11.03	60.05 ± 12.96		
40.45 ± 0.83	169.43 ± 15.31	67.08 ± 11.19		
36.37 ± 1.06	183.10 ± 16.66	71.25 ± 12.13		
29.48 ± 0.60	106.57 ± 10.81	86.10 ± 18.28		
24.72 ± 0.81	9.11 ± 5.43	112.26 ± 26.08		
19.13 ± 1.13		68.90 ± 18.01		
17.09 ± 1.18		40.96 ± 14.06		
16.81 ± 1.25		35.43 ± 10.48		
14.72 ± 1.37		12.63 ± 2.82		
13.25 ± 1.51				
9.64 ± 1.99				

3.3.8. Production of Cu-64

Cu-64 is a β+ (61.5%) and $\beta-$ (38.5%) emitter, suitable for PET imaging [5], dosimetry and possibly for therapy [12]. It has a half-life of 12.700 (2) hours and emits one gamma line at 1345.84 keV with a low branching of 0.473 (10)%.

Our data are obtained with an uncertainty of 23% in average, due to the low branching ratio of the emitted γ ray. Our results are plotted in Fig. 24. They follow the general trend and are especially in good agreement with the work of Michel et al. [45]. TALYS 1.6 Default results are in good agreement with our work.

3.3.9. Production of Ni-57

The physical characteristics of Ni-57 have been presented in part 3.2.1, and are listed in Table 6.

Our new data, plotted in Fig. 25, are in agreement with the general trend drawn by the literature data, and especially with the results of Mills et al. (1982) and the large set of data of Michel et al. [45]. The results of Williams and Fulmer [65] and Grütter, [22] are slightly lower. Those published in [21], are shifted. The effect of the recoil activity in the experimen of Shahid et al. [53] is visible in this plot. TALYS 1.6 Default is not able to reproduce the trend.

3.3.10. Production of Mn-54

The physical characteristics of Mn-54 have been stated in part 3.2.8, and are listed in Table 6.

This radionuclide is not easily detectable in the copper target due to its long half-life ($T_{1/2}$ = 312.3 (4) days) and low production cross section (see Fig. 26). All data are in good agreement, even if the results published in Grütter, [22], and Yashima et al. (2009), between 60 and 70 MeV, are slightly lower. TALYS doesn't give satisfactory results.

4. Conclusion

Experimental data have been obtained on the production of several radionuclide induced by protons on natural titanium (part 3.1), nickel (part 3.1.1) and copper (part 3.1.2). Results of this work fit with the literature and allow to add information in databases for proton induced reactions up to 70 MeV. These data have been extracted using a relative calculation through the use of monitor reactions from IAEA recommended values.

Some radionuclides produced during our experiments are of medical interest (i.e. Sc-47, Cu-64 ...). Other ones are good candidates for monitor reactions. Some new monitor reactions have been highlighted by the IAEA including Ti-nat(p,x) Sc-46, Ni-nat (p,x) Co-56,58 and Cu-nat(p,x) Co-58. Relative cross section data have been extracted in this work for these previous reactions. Ti-nat(p,x) Sc-44m,Sc-47 and Cu-nat(p,x) Ni-57,Co-57 excitation functions have a large set of data available, as well as the Ni-nat (p,x) Ni-57 and Cu-nat(p,x) Zn-62 reactions for which the recommended values could be extended up to 80 MeV.

Our data are especially in good agreement with the values published by Mills et al. in 1992 and with the large set of data published by Michel et al. in 1997. Our values contribute to the description of a large number of excitation functions. However, in the case of monitor reactions, there is a real need of absolute data. In this frame, we are currently working on a new experimental device in collaboration with the mechanical department of the SUBATECH laboratory. This device will allow stack irradiations in vacuum and will contain a Faraday cup for accurate intensity measurements. It will be placed at the end of the ARRONAX beam lines and will allow to get absolute experimental cross section data.

All data have been compared to the results of the TALYS 1.6 code using default models. TALYS shows good results for proton induced reactions on nickel. However, with copper and titanium as targets, it gives a good trend in overall but too often over- or under-estimates the cross section in comparison with the experimental values.

Acknowledgments

Authors would like to thanks all the GIP ARRONAX team and mechanical department team of SUBATECH for their contribution. The ARRONAX cyclotron is a project promoted by the Regional Council of Pays de la Loire financed by local authorities, the French government and the European Union. This work has been, in part, supported by a grant from the French National Agency for Research called 'Investissements d'Avenir', Equipex Arronax-Plus n^o ANR-11-EQPX-0004 and Labex n^o ANR-11-EQPX-0018-01.

References

[1] F.S. Al-Saleh, K.S. Al Mugren, A. Azzam, Excitation functions of (p,x) reactions on natural nickel between proton energies of 2.7 and 27.5 MeV, Appl. Radiat. Isot. 65 (1) (2007) 104–113.
[2] V.N. Aleksandrov, M.P. Semenova, V.G. Semenov, Production Cross Section of Radionuclides in (p,x) Reactions at Copper and Nickel Nuclei, Soviet. Atomic Energy 62 (6) (1987) 478–481.
[3] A.A. Alharbi, J. Alzahrani, A. Azzam, Activation cross-section measurements of some proton induced reactions on Ni, Co and Mo for proton analysis (PAA) purposes, Radiochim. Acta 99 (12) (2011) 763–770.
[4] N. Amjed, F. Tárkányi, A. Hermanne, F. Ditrói, S. Takács, M. Hussain, Activation cross-section of proton induced reactions on natural Ni up to 65 MeV, Appl. Radiat. Isot. 92 (2014) 73–84.
[5] C.J. Anderson, R. Ferdani, Copper-64 radiopharmaceuticals for PET imaging of cancer: advances in preclinical and clinical research, Cancer Biother. Radiopharm 24 (4) (2009) 379–393, http://dx.doi.org/10.1089/cbr.2009.0674.
[6] R.W. Atcher, A.M. Friedman, J.R. Huizenga, G.V. Rayudu, E.A. Silverstein, D.A. Turner, Manganese-52m, a new short-lived, generator-produced radionuclide: a potential tracer for positron tomography, J. Nucl. Med. 21 (6) (1980) 565–569.
[7] J.N. Barrandon, J.L. Debrun, A. Kohn, R.H. Spear, (É)tude du dosage de Ti, V, Cr, Fe, Ni, Cu et Zn par activation avec des protons d'énergie limitée à 20 MeV, Nucl. Instrum. Methods 127 (2) (1975) 269–278.
[8] M.E. Bennett, D.A. Mayorov, K.D. Chapkin, M.C. Alfonso, T.A. Werke, C.M. Folden, Measurement of the natLu(p,x)175Hf excitation function, Nucl. Instrum. Methods Phys. Res., Sect. B 276 (2012) 62–65.
[9] G. Blessing, W. Bräutigam, H.G. Böge, N. Gad, B. Scholten, S.M. Qaim, Internal irradiation system for excitation function measurement via the stacked-foil technique, Appl. Radiat. Isot. 955 (1995) 46–49.
[10] F. Bringas, M.T. Yamashita, I.D. Goldman, P.R. Pascholati, V. Sciani, Measurement of proton-induced reaction cross sections in Ti, Ni and Zr near the threshold, AIP Conf. Proc. 769 (1) (2005) 1374–1377, http://dx.doi.org/10.1063/1.1945260.
[11] R.L. Brodzinski, L.A. Rancitelli, J.A. Cooper, N.A. Wogman, High-energy proton spallation of titanium, Phys. Rev. C 4 (1971) 1250.
[12] J.N. Bryan, F. Jia, H. Mohsin, G. Sivaguru, C.J. Anderson, W.H. Miller, C.J. Henry, M.R. Lewis, Monoclonal antibodies for copper-64 PET dosimetry and radioimmunotherapy, Cancer Biol. Therapy 11 (12) (2011) 1001–1007.
[13] E.Z. Buthelezi, F.M. Nortier, I.W. Schroeder, Excitation functions for the production of 82Sr by proton bombardment of natRb at energies up to 100 MeV, Appl. Radiat. Isot. 64 (8) (2006) 915–924.
[14] J. De Reuck, P. Patrick Santens, K. Strijckmans, I. Lemahieu, on behalf of the european task force on age-related white matter changes. Cobalt-55 positron emission tomography in vascular dementia: significance of white matter changes, J. Neurol. Sci. 193 (2001) 1–6.
[15] C. Duchemin, A. Guertin, F. Haddad, N. Michel, V. Mëtivier, Production of medical isotopes from a thorium target irradiated by light charged particles up to 70 MeV, Phys. Med. Biol. 60 (2015) 931–946.
[16] C. Duchemin, A. Guertin, F. Haddad, N. Michel, V. Métivier, Production of scandium-44m and scandium-44g with deuterons on calcium-44: cross section measurements and production yield calculations, Phys. Med. Biol. 60 (2015) 6847–6864.
[17] L.F. Ekström, R.B. Firestone, Information extracted from the Table of Radioactive Isotopes (2004). version 2.1.
[18] D. Fink, J. Sisterson, S. Vogt, G. Herzog, J. Klein, R. Middleton, A. Koehler, A. Magliss, Production of 41Ca and K, Sc and V short-lived isotopes by the irradiation of Ti with 35 to 150 MeV protons: applications to solar cosmic ray studies, Nucl. Instrum. Methods Phys. Res., Sect. B 52 (3-4) (1990) 601–607.
[20] M. Furukawa, A. Shinohara, M. Narita, S. Kojima. Production of cosmic-ray induced radionuclides, 49V and 59,63Ni from Fe, Co and Ni irradiated with

protons up to Ep = 40 MeV, Univ.Tokyo,Inst.f.Nucl.Study, 1990, Annual Report, 1989, 32.
[21] L.R. Greenwood, K.R. Smither, Measurement of Cu spallation cross sections at lPNS, U.S. Dept.of Energy, Fusion Energy Series, vol. 18, No. 0046, 11, 1984.
[22] A. Grütter, Excitation functions for radioactive isotopes produced by proton bombardment of Cu and Al in the energy range of 16 to 70 MeV, Nucl. Phys. A 383 (1) (1982) 98–108.
[23] F. Haddad, L. Ferrer, A. Guertin, T. Carlier, N. Michel, J. Barbet, J.F. Chatal, Arronax a high-energy and high-intensity cyclotron for nuclear medicine, Eur. J. Nucl. Med. Mol. Imaging 35 (2008) 1377–1387.
[24] F.J. Haasbroek, J. Steyn, R.D. Neirinckx, G.F. Burdzik, M. Cogneau, P. Wanet. Excitation functions and thick target yields for radioisotopes induced in natural Mg, Co, Ni and Ta By medium energy protons, Council for Scientific and Industrial Research, 1976, CSIR research report FIS89, ZA7700031.
[25] A. Hermanne, F. Szelecsényi, M. Sonck, S. Takács, F. Tárkányi, P. Van den Winkel, New cross section data on68Zn(p, 2n)67Ga andnatZn(p,xn)67Ga nuclear reactions for the development of a reference data base, J. Radioanal. Nucl. Chem. 240 (2) (1999) 623–630.
[26] A. Hermanne, R. Adam Rebeles, F. Tárkányi, S. Takács, Excitation functions of proton induced reactions on natOs up to 65 MeV: experiments and comparison with results from theoretical codes, Nucl. Instrum. Methods Phys. Res., Sect. B 345 (2015) 5868. 15 February.
[27] A. Hermanne, F. Tárkányi, S. Takács, F. Ditrói, N. Amjed, Excitation functions for production of ^{46}Sc by deuteron and proton beams in ^{nat}Ti: A basis for additional monitor reactions, Nucl. Instr. Meth. Phys. Res. B 338 (1) (2014) 31–41.
[28] A. Hermanne, R. Adam Rebeles, F. Tárkányi, S. Takács, F. Ditrói, Proton and deuteron induced reactions on natGa: Experimental and calculated excitation functions, Nucl. Instrum. Methods Phys. Res. B 359 (2015) 145154.
[29] S. Huclier-Markai, A. Sabatié, S. Ribet, V. Kubicek, M. Paris, C. Vidaud, P. Hermann, C.S. Cutler, Chemical and biological evaluation of scandium(III)-polyaminopolycarboxylate complexes as potential PET agents and radiopharmaceuticals, Radiochim. Acta 99 (2011) 653–662.
[31] H. Jansen, J. Van der Naalt, A.H. Van Zomeren, A. Paans, L. Veenma-van der Duin, J.M. Hew, J. Pruim, J.M. Minderhoud, J. Korf, Cobalt-55 positron emission tomography in traumatic brain injury: a pilot study, J. Neurol. Neurosurg. Psychiatry 60 (1996) 221–224.
[32] C.U. Jost, J.R. Griswold, S.H. Bruffey, S. Mirzadeh, D.W. Stracener, C.L. Williams, Measurement of cross sections for the 232Th(p,4n)229Pa reaction at low proton energies, AIP Conf. Proc. 1525 (1) (2013) 520–524.
[33] P. Jung, Cross sections for the production of helium and long- living radioactive isotopes by protons and deuterons, Conf. Nucl. Data Sci. Technol. (1991) 352–354.
[34] M.U. Khandaker, K. Kim, M.W. Lee, K.S. Kim, G.N. Kim, Y.S. Cho, Y.O. Lee, Investigations of the natTi(p,x)43,44m,44g,46,47,48Sc,48V nuclear processes up to 40 MeV, presented at the 6th International Conference on Isotopes, Appl. Radiat. Isot. 67 (7-8) (2009) 1348–1354.
[35] M.U. Khandaker, K. Kim, M. Lee, K.S. Kim, G. Kim, Excitation functions of (p,x) reactions on natural nickel up to 40 MeV, Nucl. Instrum. Methods Phys. Res., Sect. B 269 (10) (2011) 1140–1149.
[36] R.R. Kinsey et al., The NUDAT/PCNUDAT Program for Nuclear Data, paper submitted to the 9th International Symposium of Capture Gamma-Ray Spectroscopy and Related Topics, Budapest, Hungary, October 1996. Data extracted from the NUDAT database, version 2.6.
[37] A.J. Koning, D. Rochman, Modern nuclear data evaluation with the TALYS code system, Nucl. Data Sheets, 2012, 113, 2841. TALYS 1.6 available online <http://www.talys.eu/>.
[38] P. Kopecky, Proton beam monitoring via the Cu(p, x) 58Co, 63Cu(p, 2n) 62Zn and 65Cu(p, n) 65Zn reactions in copper, Int. J. Appl. Radiat. Isot. 36 (8) (1985) 657–661.
[39] P. Kopecky, F. Szelecsényi, T. Molnár, P. Mikecz, F. Tárkányi, Excitation functions of (p, xn) reactions on natTi: monitoring of bombarding proton beams, Appl. Radiat. Isot. 44 (4) (1993) 687–692.
[40] J. Kuhnhenn, Thin target cross sections for proton-induced production of radionuclides from lead and bismuth over the proton energy range from 9 to 71 MeV, Thesis of the Universitaet Koeln, 2001, Germany.
[41] A. Majkowska-Pilip, A. Bilewicz, Complexesofscandiumradionuclidesaspre-cursors fordiagnosticandtherapeuticradiopharmaceuticals, J. Inorg. Biochem. 105 (2011) 313–320.
[42] R. Michel, G. Brinkmann, H. Weigel, W. Herr, Proton-induced reactions on titanium with energies between 13 and 45 MeV, J. Inorg. Nucl. Chem. 40 (11) (1978) 1845–1851.
[43] R. Michel, G. Brinkmann, On the depth-dependent production of radionuclides ($44 \leqslant A \leqslant 59$) by solar protons in extraterrestrial matter, J. Radioanal. Chem. 59 (2) (1980) 467–510.
[44] R. Michel, R. Stueck, F. Peiffer, Proton-induced reaction on Ti,V,Mn,Fe,Co and Ni, J. Nucl. Phys., Sect. A 441 (1985) 617.
[45] R. Michel, R. Bodemann, H. Busemann, H. Daunke, M. Gloris, H.J. Lange, B. Klug, A. Krins, I. Leya, M. Lüpke, S. Neumann, H. Reinhardt, M. Schnatz-Büttgen, U. Herpers, Th. Schiekel, F. Sudbrock, B. Holmqvist, H. Condé, P. Malmborg, M. Suter, B. Dittrich-Hannen, P.W. Kubik, H.A. Synal, D. Filges, Cross sections for the production of residual nuclides by low- and medium-energy protons from the target elements C, N, O, Mg, Al, Si, Ca, Ti, V, Mn, Fe, Co, Ni, Cu, Sr, Y, Zr, Nb, Ba and Au, Nucl. Instrum. Methods Phys. Res., Sect. B 129 (2) (1997) 153–193.
[46] S.J. Mills, G.F. Steyn, F.M. Nortier, Experimental and theoretical excitation functions of radionuclides produced in proton bombardment of copper up to 200 MeV, Int. J. Radiat. App. Instrum. Part A. Appl. Radiat. Isot. 43 (8) (1992) 1019–1030.
[47] C. Müller, M. Bunka, S. Haller, U. Köster, V. Groehn, P. Bernhardt, N. Van der Meulen, A. Türler, R. Schibli, Promising prospects for 44Sc-/47Sc-based theragnostics: application of 47Sc for radionuclide tumor therapy in mice, J. Nucl. Med. 55 (10) (2014) 1658–1664.
[48] S. Neumann, Activation experiments with medium-energy neutrons and the production of cosmogenic nuclides in extraterrestrial matter. Thesis Univ. Hannover (previously Tech. Univ. Hannover), 1999.
[49] A.L. Nichols, R. Capote, Nuclear Data for Charged-particle Monitor Reactions and Medical Isotope Productionn Summary Report of the First Research Coordination Meeting, 2013, International Atomic Energy Agency, Vienna, Austria.
[50] H. Okazawa, Y. Fujibayashi, Y. Yonekura, N. Tamaki, S. Nishizawa, Y. Magata, K. Ishizu, T. Tsuchida, N. Sadato, J. Konishi, A. Yokoyama, R. Iwata, T. Ido, Clinical application of62Zn/62Cu positron generator: Perfusion and plasma pool images in normal subjects, Ann. Nucl. Med. 9 (2) (1995) 81–87.
[51] QCALC. Data produced by the code QCALC, written by T.W. Burrows, National Nuclear Data Center, Brookhaven National Laboratory, and based on the Audi-Wapstra Atomic Mass Tables, G. Audi and A.H. Wapstra, The 1995 Update to the Atomic Mass Evaluation., 1995, Nucl. Phys. A 595, 409.
[53] M. Shahid, K. Kim, H. Naik, M. Zaman, S-C. Yanga, G. Kim, Measurement of excitation functions in proton induced reactions on natural copper from their threshold to 43 MeV, Nucl. Instrum. Methods Phys. Res., Sect. B 342 (2015) 305313.
[54] T. Siiskonen, J. Huikari, T. Haavisto, J. Bergman, S.J. Heselius, J.O. Lill, T. Lönnroth, K. Peräjärvi, Excitation functions of proton-induced reactions in natCu in the energy range 7–17 MeV, Appl. Radiat. Isot. 67 (11) (2009) 2037–2039.
[55] M. Sonck, A. Hermanne, F. Szelecsényi, S. Takács, F. Tárkányi, Study of the natNi (p,x)57Ni process up to 44 MeV for monitor purposes, Appl. Radiat. Isot. 49 (1998) 1533.
[56] F. Szelecsényi, F. Tárkányi, S. Takács, A. Hermanne, M. Sonck, Yu Shubin, M.G. Mustafa, Z. Youxiang, Excitation function for the nuclear process: Evaluation and new measurements for practical applications, Nucl. Instrum. Methods Phys. Res., Sect. B 174 (1-2) (2001) 47–64.
[57] S. Takács, F. Tárkányi, M. Sonck, A. Hermanne, New cross-sections and intercomparison of proton monitor reactions on Ti, Ni and Cu, Nucl. Instrum. Methods Phys. Res., Sect. B 188 (1-4) (2002) 106–111.
[58] F. Tárkányi, F. Szelecsenyi, P. Kopecky, Cross section data for proton, He-3 and alpha-particle induced reactions on nat-Ni, nat-Cu and nat-Ti for monitoring beam performance, in: Conf. on Nucl. Data for Sci. and Technol., Juelich, 1991, p. 529.
[59] F. Tárkányi, S. Takács, K. Gul, A. Hermanne, M.G. Mustafa, M. Nortier, P. Oblozinsky, S.M. Qaim, B. Scholten, Shubin, N. Yu, Z. Youxiang, Beam monitor reactions, in Charged Particle Cross Section Database for Medical Radioisotope Production: Diagnostic Radioisotopes and Monitor Reactions; IAEA-TECDOC-1211, 2001, pp. 49–152, IAEA, Vienna. Database available on <https://www-nds.iaea.org/medportal/>, update may 2013.
[60] Yu.E. Titarenko, V.F. Batyaev, A.Yu. Titarenko, M.A. Butko, K.V. Pavlov, S.N. Florya, R.S. Tikhonov, V.M. Zhivun, A.V. Ignatyuk, S.G. Mashnik, S. Leray, A. Boudard, J. Cugnon, D. Mancusi, Y. Yariv, K. Nishihara, N. Matsuda, H. Kumawat, G. Mank, W. Gudowski, Measurement and simulation of the cross sections for nuclide production in Nb-93 and Ni-nat targets irradiated with 0.04- to 2.6-GeV protons, Yad. Fiz. 74 (2011) 561.
[61] F.T. Tárkányi, A.L. Nichols, M-M. Be, B.V. Carlson, M. Hussain, A.V. Ignatyuk, G. Kim, F.G. Kondev, O. Lebeda, A. Luca, T. Nagai, H. Naik, M. Nortier, I. Spahn, 2012–2016. CRP on Nuclear Data for Charged-particle Monitor Reactions and Medical Isotope Production.
[62] G.J. Topping, P. Schaffer, C. Hoehr, T.J. Ruth, V. Sossi, Manganese-52 positron emission tomography tracer characterization and initial results in phantoms and in vivo, Med Phys. 40 (4) (2013) 042502, http://dx.doi.org/10.1118/1.4793756.
[62] M.S. Uddin, M. Hagiwara, F. Tárkányi, F. Ditroi, M. Baba, Experimental studies on the proton-induced activation reactions of molybdenum in the energy range 22-67 MeV, Appl. Radiat. Isot. 60 (6) (2004) 911–920.
[64] M.S. Uddin, A.K. Chakraborty, S. Spellerberg, M.A. Shariff, S. Das, M.A. Rashid, I. Ingo Spahn, S.M. Qaim, Experimental determination of proton induced reaction cross sections on natNi near threshold energy, Radiochim. Acta 104 (2016) 5, http://dx.doi.org/10.1515/ract-2015-2527.
[65] I.R. Williams, C.B. Fulmer, Excitation functions for radioactive isotopes produced by protons below 60 MeV on Al, Fe, and Cu, Phys. Rev. 162 (1967) 105.
[66] H.A. Williams, S. Robinson, P. Julyan, J. Zweit, D. Hastings, A comparison of PET imaging characteristics of various copper radioisotopes, Eur. J. Nucl. Med. Mol. Imaging 32 (12) (2005) 1473–1480.
[67] H. Yashima, Y. Uwamino, H. Sugita, T. Nakamura, S. Ito, A. Fukumura, Projectile dependence of radioactive spallation products induced in copper by high-energy heavy ions, Phys. Rev. C 66 (2002) 044607.
[68] K. Zarie, N. Al-Hammad, A. Azzam, Experimental study of excitation functions of some proton induced reactions on natTi for beam monitoring purposes, Radiochim. Acta. 94 (12) (2006) 795–799.
[69] J.F. Ziegler, M.D. Ziegler, J.P. Biersack, SRIM The stopping and range of ions in matter, Nucl. Instrum. Methods Phys. Res., Sect. B 268 (2010) 1818–1823.

Further reading

[19] FitzPeaks Gamma Analysis and Calibration Software version 3.66, produced by JF Computing Services (UK), based on methods presented in Nucl.Instrum. and Methods, 1981, 190, 89-99, describing the program SAMPO80 of the Helsinki University of Technology, Finland.

[30] IAEA, International Atomic Energy Agency. Nuclear Data Service, website: <www-nds.iaea.org/>. Last Updated: 06-January-2015.

[52] A. Ravi Shankar, N.S. Karthiselva, U. Kamachi Mudali, Thermal oxidation of titanium to improve corrosion resistance in boiling nitric acid medium, Surf. Coat. Technol. 235 (2013) 45–53.